HHS Public Access

Author manuscript

Dev Cell. Author manuscript; available in PMC 2018 March 13.

Published in final edited form as:

Dev Cell. 2017 March 13; 40(5): 491–504.e5. doi:10.1016/j.devcel.2017.02.008.

Planarian epidermal stem cells respond to positional cues to promote cell type diversity

Omri Wurtzel[1,2,3,4], **Isaac M. Oderberg**[1,2,3,4], and **Peter W. Reddien**[1,2,3,5]

[1]Whitehead Institute for Biomedical Research, Cambridge, MA 02142, USA

[2]Department of Biology, Massachusetts Institute of Technology, Cambridge, MA 02139, USA

[3]Howard Hughes Medical Institute, Chevy Chase, MD 20815, USA

Summary

Successful regeneration requires that progenitors of different lineages form the appropriate missing cell types. However, simply generating lineages is not enough. Cells produced by a particular lineage often have distinct functions depending on their position within the organism. How this occurs in regeneration is largely unexplored. In planarian regeneration, new cells arise from a proliferative cell population (neoblasts). We used the planarian epidermal lineage to study how the location of adult progenitor cells results in their acquisition of distinct functional identities. Single-cell RNA sequencing of epidermal progenitors revealed the emergence of distinct spatial identities as early in the lineage as the epidermal neoblasts, with further pre-patterning occurring in their post-mitotic migratory progeny. Establishment of dorsal-ventral epidermal identities and functions, in response to BMP signaling, required neoblasts. Our work identified positional signals that activate regionalized transcriptional programs in the stem cell population and subsequently promote cell type diversity in the epidermis.

In-Brief/eToC blurb

Wurtzel et al. examine how in planarian regeneration, adult progenitor cell location contributes to acquisition of distinct functional identities. They provide insight for how progenitors in the epidermis read their position in the animal to activating region-specific transcription, which is ultimately propagated to differentiated progeny generate the required cellular functions.

*Correspondence: reddien@wi.mit.edu.
[4]Co-first author
[5]Lead Contact

Author Contributions

OW, IMO, and PWR conceived the project and designed experiments. OW, IMO, and PWR performed all experiments. OW analyzed high-throughput sequencing data. OW, IMO, and PWR wrote the manuscript.

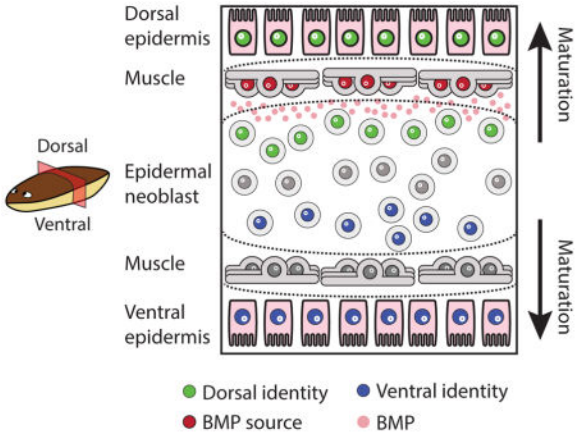

Introduction

A major challenge of adult regeneration and tissue turnover is the production of region-appropriate cell types in the absence of embryonic patterning mechanisms (Sanchez Alvarado and Yamanaka, 2014). Progenitors for regeneration, such as stem cells or dedifferentiated cells, must be regulated to choose which cell types to make, and these cell types must be appropriate for their location (Reddien, 2011). Furthermore, cells of the same lineage and cell type often have specialized functions depending on their location (Lavin et al., 2014), which requires additional control over their differentiation (Baxendale et al., 2004; Gautier et al., 2012). Therefore, mechanisms governing lineage choice and the regional specialization of cell function are of central importance in regeneration. Here, we focus on the questions of how and when region-appropriate specialization occurs within a lineage.

Planarians are free-living flatworms that use adult stem cells to maintain tissues and to regenerate (Reddien and Sanchez Alvarado, 2004). The only proliferating cell population in planarians, neoblasts, contain pluripotent stem cells (Wagner et al., 2011). Many neoblasts are specialized towards particular cell types including cells of the protonephridia (Scimone et al., 2011), intestine (Forsthoefel et al., 2012), pharynx (Adler et al., 2014; Scimone et al., 2014a), nervous system (Cowles et al., 2013; Scimone et al., 2014a), eye (Lapan and Reddien, 2012), and anterior pole (Scimone et al., 2014b). The location of a neoblast (Reddien, 2013) impacts its identity: For example, eye-specialized neoblasts are not found in the posterior of the animal (Lapan and Reddien, 2012) and intestinal neoblasts are often in proximity to the planarian gut (Wagner et al., 2011). Therefore, spatial information likely affects the identity of neoblasts and their progeny (Reddien, 2013).

Conversely, it is unknown how the spatial distribution of neoblasts and progenitors within a lineage generates a diversity of cellular identities and functions. The planarian epidermis presents an ideal system for studying this question: First, multiple cellular identities with specialized functions are found in the epidermis in specific body locations (Glazer et al., 2010; Tazaki et al., 2002), and these cells appear to emerge from a single specialized neoblast lineage (ζneoblasts; Fig 1A) (van Wolfswinkel et al., 2014). Second, there are well-

established assays for evaluating planarian epidermal integrity and function (Tu et al., 2015; van Wolfswinkel et al., 2014; Vij et al., 2012), and the status of the lineage from neoblasts (van Wolfswinkel et al., 2014) all the way to mature cells (Tu et al., 2015). Finally, the epidermal lineage has well-characterized differentiation stages (Fig 1A) that are both spatially and temporally distinct (Eisenhoffer et al., 2008; Tu et al., 2015; van Wolfswinkel et al., 2014).

The epidermal lineage is derived from mitotic ζneoblasts that are distributed throughout the mesenchyme (van Wolfswinkel et al., 2014). A ζneoblast exits the cell-cycle and progresses through a series of defined stages during its differentiation (Fig 1A) (Eisenhoffer et al., 2008; Tu et al., 2015), a process that takes at least seven days (van Wolfswinkel et al., 2014). During differentiation, cells migrate from the mesenchyme outwards to the epidermis, and ultimately integrate into the mature epidermis, a single-layered epithelial sheet (Tu et al., 2015). This is in contrast to other established models used for studying the generation of epithelial cell type diversity (Cibois et al., 2015; Dubaissi and Papalopulu, 2011; Quigley et al., 2011), such as the *Xenopus* embryonic epidermis, in which epithelial progenitors migrate from an inner monolayer to an outer monolayer. In this case, progenitors can rely on physical cell-cell communication to determine cell fates (Cibois et al., 2015; Dubaissi and Papalopulu, 2011; Quigley et al., 2011). In planarians, mesenchymal progenitors are hypothesized to rely on secreted positional cues (Reddien, 2011), creating different challenges for the generation of cell-type diversity. In this process progenitors display a stereotyped sequence of gene expression changes, collectively described as maturation (Fig 1A) (Tu et al., 2015). This apparently homogeneous population of progenitors gives rise to spatially distinct mature epidermal cell types (Glazer et al., 2010).

We devised a strategy to determine at which stage in the epidermal lineage cells express genes associated with distinct spatial identities. We developed a method for isolating dorsal and ventral epidermis, which facilitated the detection of eight spatial mature epidermal identities. We asked whether these identities emerge in the differentiated cells, their immediate progenitors, or even as early as in the spatially and temporally distant ζneoblasts that will produce these cells. The emergence of distinct expression patterns was analyzed by single-cell RNA sequencing (SCS) of 303 cells spanning every step of epidermal maturation, combined with in situ hybridization (ISH) of over 125 epidermal genes. We found that epidermal neoblasts (ζneoblasts) and progenitors from all stages of epidermal maturation express genes according to their location within the animal. Analysis of ζneoblasts and progenitors across the dorsal-ventral (DV) axis revealed divergent transcriptional programs that correlated with the emergence of distinct dorsal or ventral epidermal identities. Inhibition of *bmp4*, a dorsalizing factor (Molina et al., 2007; Orii and Watanabe, 2007; Reddien et al., 2007) that is constitutively expressed in dorsal muscle cells (Witchley et al., 2013), resulted in the rapid dorsal emergence of ventral ζneoblasts and their progeny. This lineage ventralization, following *bmp4* inhibition, did not occur in the absence of ζneoblasts even when their progeny were present. This indicates that ζneoblasts respond to positional signals in their environment and activate region-appropriate transcriptional programs. These findings demonstrate that single-cell RNA sequencing, from distinct body regions, is a powerful method for revealing the spatial identity of progenitors for regeneration and tissue maintenance. Our results demonstrate that distinct regional identities are detectable within

the neoblast population, and that signals from differentiated cells can be read by neoblasts to promote spatial cell-type diversity.

Results

Epidermal genes are expressed in at least eight different spatial patterns

Multiple cellular identities, distinguished by distinct gene expression domains, make the planarian epidermis. Our goal was to find how and when, during the formation of new epidermal cells, distinct epidermal identities emerge. Previous work identified three epidermal identities: ciliated epidermis (Glazer, 2010), non-ciliated epidermis, and dorsal-ventral (DV) boundary epidermis (Tazaki, 2002). However, other epidermal identities might exist. Since our work required a broad classification of epidermal identities, we first characterized mature epidermal identities through analysis of epidermal gene expression. We implemented an epidermal-enrichment strategy based on ammonium thiocyanate treatment (Trost et al., 2007), which allowed for the collection of the epidermis (Fig S1A; STAR Methods). Isolated epidermis was used for RNA extractions from six biological replicates from the dorsal or ventral epidermal surfaces, separately (Fig S1A–B; STAR Methods), which was followed by preparation of RNA sequencing libraries (STAR Methods). Comparison of the epidermis-enriched RNAseq libraries with libraries prepared from RNA extracted from whole worms identified 3,315 genes that were overexpressed in the epidermis (Fig 1C–E; fold-change ≥ 2; FDR < 1E-4; STAR Methods), including 393 and 233 genes enriched in either the dorsal or ventral epidermis, respectively (Fig S1D; Table S1).

We characterized the diverse patterns of epidermal gene expression by selecting 125 epidermis-enriched genes (Fig S1D–E; Table S1) and performing whole-mount in situ hybridizations with RNA probes (WISH). WISH analysis revealed that 90% (113/125) of the genes were in fact enriched in the epidermis (Fig 1B, S1F; Table S1), which we then classified to eight distinct expression patterns (Fig 1B–C; Fig S1F–G; Table S1), representing diverse mature epidermal identities (Fig 1C). We subsequently used representatives of these patterns to study when, during epidermal differentiation, spatial gene expression domains emerge.

Reconstructing the epidermal lineage by single-cell sequencing

The expression of epidermal genes can emerge before differentiation is complete (Tu et al., 2015). For example, *vim-1* was expressed in epidermal cells that were not yet integrated into the epidermis (Fig S1G), in contrast to PRSS12 and *laminB* (Fig S1G), which were expressed only in the mature epidermis. However, it is unclear how early in differentiation mature epidermal gene expression can initiate. To determine the stage of epidermal differentiation at which epidermal identities emerge, we characterized the transcriptomes of epidermal progenitors with single cell resolution. We dissected different body regions, including dorsal, ventral, or lateral tissues (Fig 1D; STAR Methods) and, following maceration of the fragments, we isolated cells by fluorescence-activated cell sorting (FACS; STAR Methods). Then, we selected cells for sequencing by quantitative PCR (qPCR) for the expression of an epidermal progenitor marker, *agat-1*, which we found to be expressed in all post-mitotic epidermal progenitors both by SCS (Wurtzel et al., 2015) and FISH (Fig S2A–

B; STAR Methods). In addition, we isolated lateral tissues and selected cells expressing an epidermal boundary marker (*laminB*; Fig 1B, S1G; (Tazaki et al., 2002)). In total, we collected 205 epidermal progenitors (*agat-1*+) and 6 epidermal boundary cells (*laminB*+). We used these cells for SCS (Picelli et al., 2014), and the data that was generated was analyzed in combination with published epidermal lineage SCS data (98 cells; (Wurtzel et al., 2015)). SCS gene expression data was visualized by t-distributed stochastic neighbor embedding (tSNE) (van der Maaten and Hinton, 2008), and the data was clustered using the Seurat package (Satija et al., 2015) (Fig 1E; Table S2; STAR Methods). The clustering analysis recapitulated known epidermal lineage cell states (Tu et al., 2015), here defined as: "ζNeoblast", "Early Stage", "Late Stage", "Later Stage", and 3 mature cell types (Fig 1E–F; S2C–F). Gene expression comparison between clusters identified 1,452 genes enriched in particular clusters (Table S3; FDR < 0.001, fold-change > 4; STAR Methods). We selected highly specific gene markers to each maturation state based on this analysis (AUC range 0.81–1; Fig 1F–G; S2C–D), and used them for FISH (Fig 1H). These data represent comprehensive gene expression profiles of every stage of planarian epidermal differentiation.

Many mature epidermal genes are expressed in Early Stage progenitors

The SCS data we collected spanned every stage of epidermal maturation, which allowed determination of whether genes expressed in the mature epidermis (Table S1), were also expressed in progenitors and at what stage. We found that 24% of these genes (Fig 2A) were expressed in at least 30% of the Early Stage or Late Stage progenitors (Table S1; STAR Methods). Interestingly, some of these genes encode proteins that are associated with mature epidermal functions, such as ciliogenesis (Fig 2B, S3A). This raised the possibility that progenitor populations display distinct epidermal identities despite having at least four days to complete their maturation (van Wolfswinkel et al., 2014). We tested these results by FISH on whole animals (Fig 2B–D; S3A–C) or by FISH on FACS-sorted cells (cell FISH; Fig S3D; STAR Methods). Expression of tested genes encoding cilia components (*e.g.* BBS1 and *ift88-like*) was detectable in Early Stage progenitors and mature epidermis (Fig 2B–D, S3A–D), but not in dividing neoblasts (Fig S3E). SCS, however, predicted that 23% of the centriole-associated genes (Azimzadeh et al., 2012) were also expressed in neoblasts (Table S4). This observation is consistent with the recent report by Duncan et al. on the expression of cilia components in neoblasts (Duncan et al., 2015). Furthermore, transcripts for 75% (20/27) of centriole-associated genes (Azimzadeh et al., 2012), which are expressed in ciliated cells (Azimzadeh et al., 2012; Wurtzel et al., 2015) were detectable in Early Stage or Late Stage progenitors (Table S4), despite the fact that cilia were restricted to the mature epidermis (Fig S3F). Therefore, cilia appeared to only be assembled in mature epidermal cells despite transcription of genes encoding cilia components in progenitors. The correlation of co-expression of multiple structural cilia genes in single cells was much higher in Later Stage progenitors compared to Early Stage or Late Stage progenitors (Average Pearson correlation r=0.08, 0.1, 0.43 for Early Stage, Late Stage, and Later Stage, respectively; STAR Methods). However, expression of cilia-encoding genes was unlikely non-specific even in Early Stage progenitors, because expression of genes encoding cilia components was completely undetectable in non-ciliated cell types, such as muscle or gut (STAR Methods; (Wurtzel et al., 2015)). These results suggest that epidermal cells can adopt

a distinct functional identity (becoming ciliated or not) early during differentiation, rather than acquiring an identity only after integration into the mature epidermis.

RNAi identifies transcription factors required for spatially-restricted epidermal identity

We observed that a number of genes with spatially-restricted expression patterns in the epidermis encode predicted transcription factors, raising the possibility that multiple transcription factors (TF) regulate epidermal spatial patterning. For instance, eight TFs were predicted to be expressed in the DV epidermal boundary cells in our SCS data (Fig 2E; STAR Methods). We validated the DV-boundary epidermis expression for seven of eight by FISH (Fig 2F, S3G). We inhibited these genes by RNAi (Fig 2G; STAR Methods) and performed FISH on regenerating heads or tails for a DV epidermal marker (*laminB*). RNAi of three genes, *Post-2a*, *Post-2b*, and BARHL1, resulted in a striking reduction of epidermal DV boundary expression (*laminB*; Fig 2G), and in addition BARHL1 RNAi also resulted in lesions around the pharyngeal cavity (Fig S3H), a region in which BARHL1 is expressed (Fig S3I). In contrast, these three TFs did not affect other mature epidermal cell types, as tested by FISH, indicating their specific requirement for activation of DV-boundary epidermis gene expression (Fig S3J). These results demonstrate that certain TFs specifically drive gene expression of epidermal subpopulations and that TFs are good subjects for study of the acquisition of spatial identity within the epidermal lineage.

Spatially-restricted epidermal identities emerge in progenitors

Mature epidermal identities have distinct spatial distributions across the different body axes (Fig 1B–C). These distinct patterns of gene expression might (1) emerge in progenitors, or (2) might only be present after cells have been incorporated into the mature epidermis. We selected epidermal TFs, which are expressed in a spatially restricted manner in the mature epidermis (Fig 1B–C, 2F, S3G), and analyzed their expression in epidermal progenitors. In the mature epidermis, *ovo-2* (Fig 1B–C, Fig 3A–B, S4A–B) was expressed in the dorsal midline and the lateral edges. Imaging a plane of internal tissues (Fig 3A–B, Fig S4B; STAR Methods) showed spatially restricted expression in immature epidermal progenitors (*agat-3*+) that was highly reminiscent of the pattern of *ovo-2* expression in the mature epidermis (Fig 1B–C, 3A). Inhibition of *wnt5*, which causes expansion of the planarian midline (Adell et al., 2009; Gurley et al., 2010), resulted in expansion of the *ovo-2* expression domain (Student's unpaired t-test $p < 0.02$; Fig S4C). In a similar fashion to *ovo-2*, *tlx-1*, which is specifically expressed in the DV boundary (Fig 2E–F, S3G), was expressed in epidermal progenitors (*agat-3*+) only next to the DV boundary and not in epidermal progenitors further away (Fig 3C–D). Furthermore, *foxJ1-4,* which is expressed in ciliated epidermis (Fig S3K), was abundantly expressed in *agat-3+* cells near ciliated epidermal regions, such as on the ventral surface (Fig 3E), but not in the vicinity of non-ciliated areas, such as the dorsal midline region (Fig 3E). Finally, we examined the spatially restricted expression of the gene DCLK2, which encodes a doublecortin protein kinase rather than a TF, and which is expressed in the ventral epidermis (Fig 1B–C). DCLK2 was expressed in multiple ventral epidermal progenitors, but not in any dorsal progenitors (Fig 3F). By contrast, the expression of DYRK4 (Fig 1B–C) was not detectable in epidermal progenitors (Fig S4D), despite having a spatially restricted expression pattern in mature cells. These results demonstrate that gene expression in immature epidermal progenitors is

pre-patterned in a manner that reflects some of the spatial identities that are found in the mature epidermis. This suggests that migratory epidermal progenitors detect their position in the animal to activate regionallyappropriate transcriptional programs that will reflect the pattern of gene expression in the mature epidermis.

Dorsal and ventral gene expression distinguishes Early Stage post-mitotic progenitors

The results above demonstrated that some genes are expressed in epidermal progenitors based on their location in the animal (Fig 3, S4B). Because the dorsal and ventral epidermis display strikingly different expression patterns (Fig 1B–C), we sought to elucidate how early during maturation dorsal and ventral identities emerge. Approaches for identifying genes that are expressed in a spatially restricted pattern within a lineage are challenging because they require comparing cells from a similar maturation stage, but from different locations. The single cells we sequenced were isolated from physically separated dorsal or ventral regions in the animal (Fig 4A), and through SCS clustering (Fig 1E–F; STAR Methods), they were assigned to a maturation stage (Fig 1E, 4A; Table S2). Therefore, this approach allows for the systematic identification of genes with spatially restricted expression in epidermal progenitors. To find the earliest differences in gene expression across epidermal populations we compared gene expression of Early Stage progenitors from dorsal and ventral regions (Fig 4A). In total, we found 23 genes that were significantly enriched (Fig 4B; Fold-change > 4; FDR < 0.1; Power > 0.4; Table S5) in dorsal or ventral progenitors, a finding that was supported by bulk RNA sequencing from dorsal or ventral animal fragments for 19/23 genes (Fig 4B). Remarkably, the expression of two genes strongly predicted whether a cell is dorsal (*PRDM1-1*; AUC = 0.85; Fig S5A; Table S5) or ventral (*kal1*; AUC = 0.9; Fig S5B; Table S5), a finding that is consistent with the whole-mount expression patterns for these genes (Fig 4C). FISH analysis validated that *prog-2*+/*PRDM1-1+* cells were restricted dorsally and that *prog-2*+/*kal1*+ were exclusively ventral (Fig 4D). Importantly, whereas *PRDM1-1* expression appeared exclusively in dorsal epidermal progenitors, *kal1* was expressed in other cell types in ventral tissues, including neural and muscle cells (Fig S5C–D), suggesting it is a broader ventral marker. The expression of *PRDM1-1* and *kal1* strongly correlated with other DV-biased identities: the majority of cells expressing *ovo-2* ($\log_2$(CPM) > 5), which is expressed only dorsally (Fig 1B–C, 3A–B), also expressed *PRDM1-1* in SCS data (Fig S5E; overlap = 67%; percentile rank of fraction overlap = 0.98; STAR Methods), but none expressed *kal1* (Fig S5E). Similarly, the expression of DCLK2 overlapped with the expression of *kal1* (Fig S5F; overlap = 35%; percentile rank of overlap = 0.84), a gene that is expressed specifically in the ventral epidermis (Fig 1B–C, 3F), but not with the expression of *PRDM1-1* (0%). These results indicate that the DV-bias observed in Early Stage gene expression is correlated with subsequent spatially restricted epidermal identities.

Epidermal neoblasts express dorsal and ventral markers

Epidermal progenitors are the product of mitotic ζneoblasts (van Wolfswinkel et al., 2014). The expression of DV-biased genes in epidermal progenitors raised the question of whether DV identities exist as early in the lineage as the ζneoblasts. We tested this possibility by analyzing the expression of DV-biased epidermal progenitor genes in neoblasts. *PRDM1-1* and *kal1* expression was highly specific to ζneoblasts in SCS data (Fig S6A), and was

detectable in 68% of the cells (Fig 5A). In addition, we used cell FISH to quantify the fraction of dividing neoblasts expressing *PRDM1-1* or *kal1*, and found that 6.7% and 9.7% of the neoblasts expressed *PRDM1-1* or *kal1*, respectively (Fig 5B). Similarly, we quantified the proportion of ζneoblasts in the dividing neoblast pool by cell FISH and found that they comprised 31% of dividing neoblasts (Fig S6B). Therefore, we estimated that ~53% of ζneoblasts express either *PRDM1-1* or *kal1* using cell FISH. Strikingly, the expression of *PRDM1-1* and *kal1* in SCS was mutually exclusive in ζneoblasts (Fig 5A), a finding we corroborated with cell FISH on dividing neoblasts (Fig S6C; number of cells counted = 1061).

We examined the spatial distribution of *PRDM1-1+* ζneoblasts by whole-mount FISH, and detected them only on the dorsal side (Fig 5C). Conversely, *kal1+* ζneoblasts were found only ventrally (Fig 5C, S6D). We quantified the positions of *kal1+* neoblasts along the DV axis by imaging transverse sections (Fig 5D, S6E), which were labeled for major anatomical structures (intestine, *madt* (Wenemoser and Reddien, 2010); and DV-boundary epidermis, *laminB*). *kal1+* cells were always ventral to the intestine or next to the DV-boundary epidermis (Fig 5D–E). We divided each transverse section into 10 regions along the DV axis and counted the number of *kal1+* neoblasts in each region (Fig 5E; STAR Methods). The majority (79%) of the *kal1+* neoblasts were found in the two regions above the ventral epidermis (Fig 5E), and notably *kal1+* neoblasts were not found in any of the dorsal regions. Utilizing ζneoblast markers, we found that *kal1+* ζneoblasts were closer to the ventral epidermis, and that ζneoblasts more internally did not express *kal1* (Fig 5F, S6F). These findings show that *kal1* expression in neoblasts is correlated to the position of the cells across the DV axis. To further confirm these results, we isolated groups of 500 dividing neoblasts by FACS from either dorsal or ventral planarian fragments. We performed qPCR analysis on eight dorsal and six ventral neoblast groups (STAR Methods) and found that in dividing neoblasts, *PRDM1-1* was significantly overexpressed on the dorsal side, and by contrast, *kal1* was significantly overexpressed on the ventral side (Fig 5F). These findings demonstrate that gene expression in neoblasts within a lineage reflects their position in the animal. This positional identity is likely subsequently propagated to the spatially divergent epidermal progenitors, which ultimately generate regionally appropriate mature epidermal cells.

The BMP signaling gradient affects the DV identity of ζneoblasts and epidermal progenitors

The dorsal and ventral identities found in ζneoblasts raised the possibility that ζneoblasts respond to an extracellular signal to activate position-specific transcriptional programs. In planarians, many genes regulating adult patterning are expressed in muscle cells (Witchley et al., 2013), but the connection between patterning gene expression in muscle and neoblast states is poorly understood. *bmp4* expression from dorsal muscle cells (Witchley et al., 2013) regulates the polarization of the DV axis (Molina et al., 2007; Orii and Watanabe, 2007; Reddien et al., 2007), and thus it is an attractive candidate for regulating the emergence of DV identities in ζneoblasts. Importantly, the expression of *kal1* was spatially opposed to *bmp4* expression (Fig 5D). *bmp4* inhibition leads to progressive ventralization of the animals (Molina et al., 2007; Orii and Watanabe, 2007; Reddien et al., 2007), resulting in

ventral features appearing dorsally. We assessed if BMP signaling actively represses the expression of ventral epidermal genes in dorsal epidermal lineage cells. We inhibited *bmp4* and examined *kal1* expression in two scenarios (Fig 6A; STAR Methods). First, in intact animals, 10 days following *bmp4* inhibition, a time-point at which animals appeared indistinguishable from controls (Fig 6A) and; second, in regenerating animals, 10 days following amputation, and a total of 20 days after initiating *bmp4* inhibition. In this condition, the animals displayed major morphological defects reflecting ventralization of the regenerating tissue (Fig 6A). Following RNAi, *kal1*+ cells were found dorsally in *bmp4* RNAi animals (Fig 6B), but never dorsally in controls (Fig 6B). Importantly, *kal1*+ Early Stage progenitors (*prog-2*+) were present dorsally in both intact and regenerating *bmp4* RNAi animals (Fig 6B). Furthermore, *kal1+* ζneoblasts were detectable in *bmp4* RNAi animals dorsally (Fig 6C) 10 days from the beginning of the experiment, suggesting that proximity to a BMP source represses the ventral ζneoblast identity.

Neoblasts are required for responding to changes in BMP signaling

The outcome of *bmp4* RNAi on epidermal lineage cells at their various stages, ventralization, could result from a response only in neoblasts, which produce the lineage, or a response in neoblasts and post-mitotic cells of the lineage. To distinguish between these possibilities, we tested whether ventralization of the epidermal lineage following *bmp4* RNAi required neoblasts. Animals were split into two groups (Fig 6D), with the first group lethally irradiated on day zero and the second unirradiated. Lethal irradiation ablates all neoblasts by 24 hours post-irradiation but post-mitotic epidermal progenitors persist for up to 6 days as they transit towards differentiation (Eisenhoffer et al., 2008). At 24 hours post-irradiation, half of each group was injected with *bmp4* or control dsRNA. At four, six, or eight days following injection animals were fixed and analyzed for the expression of *kal1* by FISH (Fig 6E–I). Numerous ectopic *kal1*+ progenitors were present in unirradiated *bmp4* RNAi animals, at all time points examined (Fig 6E–F, S7A). Moreover, *kal1* expression in the mature dorsal epidermis was detected eight days following injection (Fig 6G). By contrast, we did not detect *kal1* expression in progenitors or mature epidermal cells on the dorsal side of animals that were irradiated prior to *bmp4* inhibition (Fig 6E–I). Next, we examined the expression of *rootletin*, which is normally spatially restricted to dorsal epidermis and expressed ubiquitously in ventral epidermis (Fig S7B). Dorsal expression of *rootletin* was expanded and resembled the ventral side in 3/8 unirradiated *bmp4* injected animals (Fig 6G). This transformation did not occur in animals that were irradiated prior to the injection (100%; Fig 6G). Finally, we quantified the number of dorsal *kal1*+ cells, and confirmed our observations that ectopic *kal1* expression was only present in unirradiated animals following *bmp4* inhibition (Fig 6H–I). These findings suggest that within the epidermal lineage, it is primarily ζneoblasts that respond to BMP signaling. Finally, we examined the spatial distribution of the ectopic *kal1*+ cells following *bmp4* RNAi by imaging transverse sections of unirradiated *bmp4* and control RNAi animals (Fig 6J). We found, in all affected animals, that ectopic *kal1*+ cells appeared only near the dorsal epidermis, and not in the interior of the animal (Fig 6J). Since we observed (Fig 5F, S6F) that *kal1*+ ζneoblasts are generally closer to the epidermal surface than *kal1*-ζneoblasts, this result indicates that *kal1* expression is dependent not only on DV position, but also on proximity to the periphery of the animal, which might indicate a more mature cell state that

responds to BMP levels. Therefore, we suggest that ζneoblasts sense the BMP levels in their environment and obtain a DV spatial identity, promoting cell type diversity to form region-appropriate epidermis.

Discussion

The body plan of even relatively simple animals is constructed of diverse, spatially arranged cell types. Adult planarians can replace all cell types during tissue turnover or regeneration through neoblast differentiation and integration of their progeny into organs and tissues (Reddien and Sanchez Alvarado, 2004). Therefore, the molecular signals that specify neoblasts and their descendants towards the appropriate cell types are important for understanding tissue turnover and regeneration. Equally important is understanding how cells within a particular lineage acquire unique functions based on their position in the animal (Lavin et al., 2014). These functions are often essential for basic activities. For example, the production of spatially arranged ciliated epidermis is essential for normal planarian motility (Glazer et al., 2010). A major challenge in identifying regulators of this process is that cell population-scale analyses often utilize cells that are heterogeneous with regards to cell type, differentiation state, and location within the animal. Therefore, single-cell analyses are highly advantageous for studying where, when, and how specialization emerges within a cell population.

Expression of spatially restricted epidermal identities in the epidermal lineage

We used the planarian epidermis to study the location, timing, and mechanism of spatially restricted epidermal identity acquisition during differentiation (Fig 7). We first characterized the different spatiallyrestricted identities that are found in the epidermis and then analyzed, using SCS and FISH, the transcriptomes of epidermal progenitors from throughout the lineage. We identified transcriptional programs that were dependent on the position of the cell within the animal (Fig 7A–B). Importantly, position-specific gene expression for different identities emerged at different stages of maturation. For example, the spatially restricted expression of DYRK4 (Fig 1B–C, S4D) was detectable only in the mature epidermis. The expression of *ovo-2*, on the other hand, could be found both in the mature epidermis and in a pattern similar to its ultimate epidermal pattern in migratory, mesenchymal, Late Stage progenitors (Fig 1B–C, Fig 3E). The expression of genes encoding cilia components was observed by FISH in Early Stage progenitors (Fig 2B–C, Table S4), and SCS suggested that some cilia components were already expressed in neoblasts (Table S4). In fact, Duncan et al. reported recently that some cilia components, such as *cfap53* and *rsph6A*, are expressed in neoblasts, suggesting that cilia specification might occur in mitotic cells (Duncan et al., 2015). Importantly, DV-restricted gene expression was found even at the top of the epidermal lineage, in ζneoblasts (Fig 7C), which have at least eight days and multiple stages to transit before they have fully matured and migrated to their final destination (van Wolfswinkel et al., 2014).

The epidermis is a model for generation of regionally appropriate cell types

Planarian epidermal progenitors have been studied in multiple reports, with findings focusing on phases of epidermal maturation (Eisenhoffer et al., 2008; Tu et al., 2015; van

Wolfswinkel et al., 2014; Zhu et al., 2015). Less emphasis has been given to the distinct cellular identities individual cells can acquire, and the spatiotemporal regulation of these distinct identities.

The emergence of distinct gene expression domains in the planarian epidermis (e.g. *ovo-2* and DYRK4 at the dorsal epidermis; *laminB* in the DV boundary; DCLK2 at the ventral epidermis; Fig 1B–C) is very likely regulated by multiple mechanisms. Our analysis demonstrated that patterning molecules, such as BMP (Molina et al., 2011; Reddien et al., 2007) and Wnt5 (Adell et al., 2009) were essential for the normal formation of some of these patterns. Interestingly, the major source of these factors is muscle cells at distinct regions of the animal (Witchley et al., 2013). We hypothesize that progenitors for regeneration and tissue-maintenance sense the levels of patterning factors at their location, and respond by activating a region-appropriate transcriptional program. This hypothesis is consistent with several observations made on regional gene expression in planarians: First, patterning molecules are constitutively expressed in planarians (Reddien, 2011); second, RNAi of these molecules leads to patterning defects in intact and regenerating animals (Reddien, 2011), and finally, with the rapid establishment of regionally-appropriate gene expression of patterning factors following injuries, prior to the generation of regionally-appropriate cell types (Gurley et al., 2010; Petersen and Reddien, 2009; Witchley et al., 2013; Wurtzel et al., 2015). Importantly, it has been unclear at what stage of differentiation cells respond to these signals, and in particular whether it is mature cell types, post-mitotic progenitors, and/or neoblasts that respond.

DV gene expression distinguishes populations of epidermal progenitors and ζneoblasts

To identify the cells that respond to positional cues, we first searched for the earliest discernable transcriptional differences between spatially distinct epidermal lineage cells. Using SCS on samples obtained from dorsal or ventral regions, we identified 23 genes that were potentially expressed in a regionally restricted manner at a very early stage of differentiation. Remarkably, the expression of two genes was sufficient to identify the DV-location of the vast majority of Early Progenitors (*PRDM1-1* for dorsal cells and *kal1* for ventral cells). Furthermore, these genes were expressed in spatially divergent epidermal neoblast populations, as observed by FISH, SCS, and qPCR analysis. These results demonstrated that ζneoblasts are heterogeneous in a manner that is explained best by their position within the animal (Fig 7C–D), which suggests that ζneoblasts can respond to positional cues.

Neoblasts respond to BMP levels by acquiring a DV-positional identity

One positional cue, *bmp4*, is expressed from dorsal muscle cells (Witchley et al., 2013) in a gradient that is strongest at the midline. It promotes acquisition of dorsal tissue identities, and its inhibition causes progressive ventralization of the animal (Molina et al., 2007; Orii and Watanabe, 2007; Reddien et al., 2007). Strikingly, following a short *bmp4* RNAi treatment, expression of a ventral gene (*kal1*) appeared dorsally in epidermal neoblasts and their progeny. Regions in the dorsal epidermis, normally devoid of cilia, co-expressed *kal1* and *rootletin* in these *bmp4(RNAi)* animals, indicating that some ectopic *kal1*+ cells adopted a ventral functional identity. Importantly, *kal1*+ ζneoblasts were largely found closer to the

epidermal surface than *kal1*-ζneoblasts, indicating that *kal1* expression is dependent not only on DV position but also on proximity to the periphery of the animal. This might indicate that as ζneoblasts move peripherally, they mature to a cell state that responds to patterning signals.

Following ablation of neoblasts by lethal irradiation, however, *bmp4* inhibition did not result in dorsal expression of *kal1* or in ectopic *rootletin* expression. Therefore, our data suggest that it is the neoblasts that are primarily capable of adopting ectopic ventral identities in response to BMP inhibition, which were then propagated to their progeny. Furthermore, this suggests that mature epidermal identities are not plastic even in response to changes in the BMP signaling environment.

Because *bmp4* is expressed largely exclusively in dorsal muscle cells (Witchley et al., 2013), we suggest that neoblasts read a BMP gradient established by dorsal muscle, and respond by activating a DV-appropriate transcriptional program, which subsequently generates the correct types of epidermis (Fig 7B–D). Planarian regeneration requires two components: collectively pluripotent neoblasts (Adler and Sanchez Alvarado, 2015; Reddien, 2013), which are the cellular source for all new tissues, and a set of positional signals (Reddien, 2011), which are expressed from muscle cells (Witchley et al., 2013), that provide the patterning information required for regeneration. Our results support a model in which neoblasts, within a lineage, respond directly to the muscle-derived positional signals in order to produce the required regionally appropriate cell types. This model helps explain how planarians maintain a complex body plan during tissue turnover and in response to injury.

STAR Methods

KEY RESOURCES TABLE

REAGENT or RESOURCE	SOURCE	IDENTIFIER
Antibodies		
Anti-Digoxigenin-AP, Fab fragments	Sigma Aldrich	Cat#11093274910
Anti-Digoxigenin-POD (poly), Fab fragments	Sigma Aldrich	Cat#11633716001
Anti-Fluorescein-AP, Fab fragments	Sigma Aldrich	Cat#11426338910
Anti-DNP HRP Conjugate	Sigma Aldrich	Cat#FP1129
Mouse monoclonal anti-acetylated Tubulin	Sigma Aldrich	Cat#T7451
Goat Anti-Mouse IgG H&L (HRP)	Abcam	Cat#ab6789
Bacterial and Virus Strains		
Escherichia coli DH10B	Invitrogen	Cat#18297010
Biological Samples		
N/A	N/A	N/A
Chemicals, Peptides, and Recombinant Proteins		
Ammonium thiocyanate	Sigma Aldrich	Cat#221988
TRIzol	ThermoFisher Scientific, Inc.	Cat#15596018
Buffer TCL	QIAGEN, inc.	Cat#1031576

REAGENT or RESOURCE	SOURCE	IDENTIFIER
Western Blocking Reagent	Roche	Cat#11921673001
Critical Commercial Assays		
TruSeq RNA library prep kit V2	Illumina, Inc.	Cat#RS-122-2001/2
Nextera XT	Illumina, Inc.	Cat#FC-131-1096
KAPA HiFi HotStart PCR ReadyMix	Kapa Biosystems	Cat#KK2602
High Sensitivity DNA Qubit kit	Life Technologies	Cat#Q32854
Deposited Data		
Sequencing data (single-cell RNA sequencing and RNA sequencing); Accession PRJNA353867	This paper	http://www.ncbi.nlm.nih.gov/bioproject/353867
S. mediterranea transcriptome assembly (dd_v4)	Liu et al., 2013	http://planmine.mpi-cbg.de/
Experimental Models: Cell Lines		
N/A	N/A	N/A
Experimental Models: Organisms/Strains		
Schmidtea mediterranea, asexual	Reddien lab	N/A
Oligonucleotides		
Primer for qPCR for *agat-1* (fw): CCTAAAAGGCGAAGGTGTGACT	This paper	N/A
Primer for qPCR for *agat-1* (rev): TGCAACATCCAAACCGACAGA	This paper	N/A
Primer for qPCR for l*aminB* (fw): TGTGGGTAGCCTTTTCTTCTCCC	This paper	N/A
Primer for qPCR for *laminB* (rev): CGCAAGGTTCAGGTGATCCG	This paper	N/A
Primer for qPCR for *kal1* (fw): TCTGTGTGCCCTCTTGTACG	This paper	N/A
Primer for qPCR for *kal1* (rev): CAGATTTTCCGGCTGAGAAG	This paper	N/A
Primer for qPCR for *PRDM1-1* (fw): CGGTGAACGACCTTTCAAGT	This paper	N/A
Primer for qPCR for *PRDM1-1* (rev): TCAAACAAACCGAACACTCG	This paper	N/A
Primer for qPCR for *smedwi-1* (fw): GTCTCAGAAAACAACTAAAGGTACAGCA	van Wolfswinkel et al., 2014	N/A
Primer for qPCR for *smedwi-1* (rev): TGCTGCAATACACTCGGAGACA	van Wolfswinkel et al., 2014	N/A
Recombinant DNA		
pGEM-T easy vector system	Promega	https://www.promega.com/products/pcr/pcr-cloning/pgem_t-easy-ve
Software and Algorithms		
R v3.2.3	The R Foundation	https://www.r-project.org/
edgeR v3.6.8	Robinson et al., 2010	https://bioconductor.org/packages/release/bioc/html/edgeR.html
bedtools v2.20.1	Quinlan and Hall, 2010	http://quinlanlab.org/tutorials/bedtools/bedtools.html
novoalign v2.08.02	NovoCraft Technologies	http://www.novocraft.com/products/novoalign/
mafft v7.017b	Katoh et al., 2009	http://mafft.cbrc.jp/alignment/software/

REAGENT or RESOURCE	SOURCE	IDENTIFIER
Seurat v1.2	Satija et al., 2015	http://satijalab.org/seurat/
RaXMLv7.2.6	Stamatakis. 2006	http://sco.h-its.org/exelixis/software.html
PANTHER v11	Mi et al., 2016	http://www.pantherdb.org/tools/hmmScoreForm.jsp
BLAST+ v2.4.0	Camacho et al., 2009	https://blast.ncbi.nlm.nih.gov
FIJI/ImageJ v1.51d	Schindelin et al., 2012	http://imagej.net/Fiji
Other		
Planarian Single cell RNA sequencing resource	Wurtzel et al., 2015	https://radiant.wi.mit.edu/
Mapping of labels in figure to contig IDs in transcriptome assembly	This paper, Table S6	N/A

CONTACT FOR REAGENT AND RESOURCE SHARING

Further information and requests for resources and reagents should be directed to the Lead Contact, Peter W. Reddien (reddien@wi.mit.edu).

EXPERIMENTAL MODEL AND SUBJECT DETAILS

For all experiments, a clonal strain of asexual *Schmidtea mediterranea* was used. Animals were cultured at 20°C in the dark and were fed weekly with beef liver. Prior to gene inhibition experiments animals were starved for 7 days.

METHOD DETAILS

Gene labeling and nomenclature—Previously published planarian genes, and genes for which we performed phylogenetic (*PRDM1-1*, *ovo-2*, *ovo-3*) or domain-structure analysis (*kal1*) appear in *italics* throughout the text and the figures. Uppercase labels are the human best-blast hits (blastx; E-value < 10^{-5}; (Camacho et al., 2009)), or genes not named with detailed analysis (such as phylogenetic analysis). Numeric labels with “dd_” prefix are shown for genes without human best-blast hit; instead the contig id in the dd_v4 transcriptome assembly was used (Liu et al., 2013). Mapping of gene labels in figures to contig ids is found in Table S6.

Planarian epidermis isolation and RNAseq library preparation—Uninjured and injured (3 hours post amputation) animals were used for epidermis extraction separately. Epidermal cells were isolated by incubating planarians in a solution of 3.8% Ammonium Thiocyanate [Sigma-Aldrich 221988-100G] as previously described (Trost et al, 2007) in phosphate-buffered saline (PBS) for 20 minutes. The dorsal or ventral epidermal cells were scraped off the worms, separately, with a needle pulled from a borosilicate glass capillary [Sutter Instrument Co. B100-75-15]. Epidermal cells were transferred into a collection tube on ice. Cells were spun down at 300G for 5 minutes at 4°C, resuspended in PBS, and spun down again. Cells were resuspended in 0.25 mL of TRIzol (ThermoFisher Scientific Inc. #15596018) and stored at −80°C. In parallel, whole animal controls were put in TRIzol. RNA extraction for samples in TRIzol was performed according to manufacturer’s protocol. For each sample, 1 μg of RNA was used for RNA sequencing library preparation using the

TruSeq RNA library prep kit V2 (Illumina, Inc., Cat#RS-122-2001/2) following the manufacturer's protocol. Libraries were sequenced on Illumina HiSeq.

Differential expression analysis of epidermis-enriched RNAseq libraries— Sequenced RNA-seq libraries were mapped as recently described (Wurtzel et al., 2015) using Novoalign v2.08.02 with parameters [-o SAM -r Random] to the *S. mediterranea* dd_Smed_v4 transcriptome assembly (Liu et al., 2013). Read count per contig was calculated with bedtools v2.20.1 (Quinlan and Hall, 2010) for each library. Short contigs (<350) were removed from further analysis, and reads mapped to different contig isoforms summed to represent a single contig. Differentially expressed genes were called using EdgeR v3.6.8 (Robinson et al., 2010), requiring minimal fold-change of 2 and FDR smaller than 1E-4.

Single-cell collection by FACS and qPCR—Animals were subjected to 2 transverse amputations to generate pre-pharyngeal fragments. The fragments were further dissected into dorsal, ventral, and lateral fragments (Fig 2A). Samples were macerated, stained with Hoechst (1:25) and propidium iodide (1:500), and 2C cells were sorted to plates containing lysis buffer (TCL buffer; QIAgen, inc.), as recently described (Wurtzel et al., 2015). Following reverse transcription and cDNA amplification (Picelli et al., 2013; Wurtzel et al., 2015), qPCR was performed on plates (total 1,096 cells) to identify and isolate *agat-1* expressing cells (forward and reverse sequences, CCTAAAAGGCGAAGGTGTGACT and TGCAACATCCAAACCGACAGA, respectively), with the following program [95°C (30s), 40 cycles (95°C 3s, 60°C 30s)]. Similarly, cells from the lateral region were also screened for the expression of the dorsal-ventral (DV) epidermal boundary marker *laminB* (forward and reverse sequences, TGTGGGTAGCCTTTTCTTCTCCC and CGCAAGGTTCAGGTGATCCG, respectively). Cells displaying Ct value of 25 or less were considered as expressing the assayed gene and were selected for single-cell RNA sequencing (SCS) library preparation.

Single-cell RNA sequencing library preparation—Libraries were prepared following a published protocol (Picelli et al., 2014) with previously described modifications (Wurtzel et al., 2015).

In Situ Hybridizations—Nitroblue tetrazolium/5-bromo-4-chloro-3-indolyl phosphate (NBT/BCIP) colorimetric whole-mount in situ hybridizations (ISH) were performed as previously described (Pearson et al. 2009). Fluorescence in situ hybridizations (FISH) were performed as previously described (King and Newmark 2013) with minor modifications. Briefly, animals were killed in 5% NAC and treated with proteinase K (2 μg/ml). Following overnight hybridizations, samples were washed twice in each of pre-hybridization buffer, 1:1 pre-hybridization-2X SSC, 2X SSC, 0.2X SSC, PBS with Triton-X (PBST). Subsequently, blocking was performed in 0.5% Western Blocking Reagent (Roche, 11921673001) and 5% inactivated horse serum PBST solution when anti-DIG or anti-DNP antibodies were used, and in in 1% Western Blocking Reagent PBST solution when an anti-FITC antibody was used. Post-antibody binding washes and tyramide development were performed as described

(King and Newmark 2013). Peroxidase inactivation with 1% sodium azide was done for 90 minutes at room temperature.

Immunostainings—Immunostainings for acetylated-tubulin were performed as previously described (Reddien et al., 2007). Immunofluorescence (IF) and fluorescent in situ hybridization (FISH) signals were developed using tyramide conjugated fluorophores generated from AMCA, fluorescein, rhodamine (Pierce), and Cy5 (GE Healthcare) N-hydroxysuccinimide (NHS) esters as previously reported (Hopman et al., 1998).

Irradiation—Animals were irradiated using Gammacell 40 dual ^{137}cesium sources (6000 rads) and were used for experiments 24 hours following irradiation, when all neoblasts are ablated (Eisenhoffer et al., 2008).

Gene cloning and transformation—Genes were cloned as previously described (Wurtzel et al., 2015). Briefly, gene-specific primers were used to amplify gene sequences of planarian cDNA. Amplified sequences were cloned into pGEM vectors following the manufacturer's protocol (Promega), and transformed to *E. coli* DH10B by heat-shock. Bacteria were plated on agarose plates containing 1:500 carbenicillin, 1:200 Isopropylthio-b-D-galactoside (IPTG), and 1:625 5-bromo-4-chloro-3-indolyl-β-D-galactopyranoside (X-gal) for overnight growth. Colonies were screened by colony PCR and gel electrophoresis. Plasmids were extracted from positive colonies and subsequently validated by Sanger-sequencing (Genewiz, Inc.).

Double-stranded RNA synthesis and RNAi experiments—Gene inhibition was done by feeding the animals with dsRNA corresponding to the target gene. dsRNA was synthesized as previously described (Wurtzel et al., 2015) following a published protocol (Rouhana et al., 2013). Animals were starved for 7 days prior to experiments and were kept in the dark for at least 2 hours before each feeding. Animals were fed 6 times, unless stated otherwise, every 3 days by mixing the dsRNA with homogenized beef liver (1:3). Following the RNAi feedings, animals were cut and allowed to regenerate for 8 days, while being monitored for defects. Following the 8-day recovery period, animals were fixed and analyzed by FISH. dsRNA injections, using Drummond Nanoject II, were performed in the prepharyngeal region. *bmp4* inhibition by injection was performed using a single injection.

Isolation of cells by FACS for Cell FISH—Cell suspension was prepared from whole animals or from fragments as recently described (Wurtzel et al., 2015). FACS gating was performed for previously described cell populations (Hayashi et al., 2006).

qPCR of dividing neoblasts isolated from dorsal or ventral regions—Animals were cut transversely and then dorsal and ventral fragments were isolated. Fragments from different animals were pooled (>20) and macerated to a single cell suspension, as recently described (Wurtzel et al., 2015). Groups of 500 dividing neoblasts, from the dorsal and ventral samples, were sorted using a flow cytometer, separately (dorsal replicates: n = 8; ventral replicates: n = 6) into plates containing 30 μl of lysis buffer (TCL buffer; QIAgen, inc.). RNA from samples was converted to cDNA and amplified using the Smart-seq V2 (Picelli et al., 2013) protocol with minor modifications (Wurtzel et al., 2015). The amplified

cDNA library concentrations were measured using Qubit fluorometer (Life Technologies; Q32854) and sample concentrations were normalized to 5 ng/μl. Expression of the target genes was measured in each sample using qPCR. qPCR was performed using the Applied Biosystems 7500-fast RT-PCR machine for *smedwi-1* (forward and reverse primer sequences: GTCTCAGAAAACAACTAAAGGTACAGCA and TGCTGCAATACACTCGGAGACA, respectively), *PRDM1-1* (forward and reverse primer sequences: CGGTGAACGACCTTTCAAGT and TCAAACAAACCGAACACTCG, respectively), and *kal1* (forward and reverse primer sequences: TCTGTGTGCCCTCTTGTACG and CAGATTTTCCGGCTGAGAAG, respectively) with the following program [95°C (30s), 40 cycles (95°C 3s, 60°C 30s)], with at least two technical replicates per sample. The measured Ct values of either *kal1* or *PRDM1-1* were normalized by the sample expression of *smedwi-1*, a pan-expressed neoblast gene (Reddien et al., 2005). Student t-test was used for differential expression analysis of between dorsal- and ventral-isolated samples, and p values were corrected for multiple hypothesis testing using the Bonferroni correction.

Analysis of single cell RNA sequencing data—Gene expression data were mapped to the dd_Smed_v4 assembly (Liu et al., 2013) as previously described (Wurtzel et al., 2015). Recently published SCS data (Wurtzel et al., 2015) prepared using the same protocol and equipment, was combined if the cells were from the epidermal lineage. Gene expression data for all cells were processed together as follows: Following mapping using Novoalign v2.08.02, a raw expression matrix was generated using custom Perl script, and expression matrix was normalized using edgeR v3.6.8 (Robinson et al., 2010). Contigs shorter than 450 nt were removed. Cells expressing less than 1000 or more than 7800 genes were removed from further analysis to ensure low-quality cells, or potentially contaminated samples were not included in the analysis (Wurtzel et al., 2015). Initial determination of significant principal components was performed by calling function mean.var.plot with parameters [y.cutoff = 2.5, x.low.cutoff = 2, fxn.x = expMean,fxn.y = logVarDivMean], which found 267 genes meeting these criteria. The jackstraw function [num.replicate = 200] determined principal components 1–12 as significantly contributing to cell-to-cell gene expression variance. The function pca.sig.genes was called with parameters [pcs.use = 1:12, pval.cut = 1e-5, max.per.pc = 300] and the resultant list was used for a second principal component analysis (PCA) analysis. Then, four cells were removed from the dataset [“D15.101224_DMX”, “D15.101225_DMX”, “D15.101162_DLX”, “D15.101359_L0X”], as they expressed multiple neural genes (including *PC2*, *synapsin*, and *synaptotagmin*), and were unlikely to be part of the epidermal lineage. tSNE was performed using the function run_tsne [dims.use = c(1:18), perplexity = 20, do.fast = T]. Next, data was clustered by DBclust_dimension [reduction.use = “tsne”, G.use = 2, set.ident = TRUE, MinPts = 3] and clusters were sorted by the buildClusterTree function [do.reorder = TRUE, reorder.numeric = TRUE, pcs.use = 1:18]. Following gene expression analysis, cluster 3 was determined to represent muscle cells, based on expression of multiple muscle markers, and was removed. Clusters 8, 11 and 12 included small number of low complexity cells and were removed as well.

Contig selection for calculating gene expression correlation—The transcriptome assembly was searched for contigs with best-blast hit description including the keywords IFT or “intraflagellar transport”. The expression of all contigs was visualized using the SCS resource (Wurtzel et al., 2015) and genes that were not exclusively expressed in ciliated cells (e.g. epidermal cells, protonephridia, ciliated neurons) were discarded. For each gene pair, Pearson correlation (r) was calculated, per cluster, and then z-transformed using Fisher z-transformation. Average was calculated on z-transformed values, per cluster, and then transformed to r.

Contig	Best Blast hit description	ID	E-value	Organism
dd_Smed_v4_10638_0_1	IFT172-like protein	GQ337484.1	0	Smed
dd_Smed_v4_11300_0_1	intraflagellar transport 140 homolog (Chlamydomonas) (IFT140)	uc002cmb.3	0	Human
dd_Smed_v4_5043_0_1	IFT52-like protein	GQ337481.1	0	Smed
dd_Smed_v4_5484_0_1	IFT88-like protein	GQ337482.1	0	Smed
dd_Smed_v4_7099_0_1	intraflagellar transport 57 homolog (Chlamydomonas) (IFT57)	uc003dwx.4	3.00E-91	Human
dd_Smed_v4_7533_0_1	intraflagellar transport 172 homolog (Chlamydomonas) (IFT172)	uc002rku.3	1.00E-53	Human
dd_Smed_v4_8803_0_1	intraflagellar transport 81 homolog (Chlamydomonas) (IFT81)	uc001tqh.3	0	Human
dd_Smed_v4_9110_0_1	intraflagellar transport 80 homolog (Chlamydomonas) (IFT80)	uc021xgr.1	0	Human

Identification of DV-boundary epidermis transcription factors—TFs that were overexpressed in the epidermal lineage were collected from three datasets: (1) TFs enriched in one or more epidermal progenitor or mature epidermis cluster when compared to previously published SCS gene expression of other cell types (Wurtzel et al., 2015), using the Seurat v1.2 package (Satija et al., 2015) find.markers function with thresholds: [FDR < 1E-3, FC > 2]; (2) TFs that were overexpressed in bulk epidermal RNA-seq compared to whole-worm controls [FDR < 0.01, FC > 2]; or (3) that were downregulated in animals with depleted epidermal lineage (*zfp-1* RNAi) using recently published RNAseq data (van Wolfswinkel et al., 2014) that were mapped to the dd transcriptome (Liu et al., 2013) and analyzed using the same approach described for the bulk epidermal RNAseq libraries data analysis with the following thresholds for significance (FDR < 0.01, FC > 2). TFs enriched in the DV boundary epidermis SCS data (Table S3) or expressed in at least half of the DV-boundary epidermis cells but in none of the other mature cell types (Fig 2E) were further analyzed by FISH and RNAi.

Microscopy and image analysis—FISH and IF images were collected using a confocal microscope (Zeiss LSM 700). Cell counting was performed using FIJI/ImageJ v1.51d (Schindelin et al., 2012) by cropping images to a set size and counting cells using the “Cell Counter” component. The same region was used to count cells for both the controls and the experiment. Transverse sections were generated by using a scalpel and generating two transverse cuts. Measurement of spatial distribution of *kal1*+ neoblasts (Fig 5D) was done by imaging transverse sections, dividing each section into 10 segments of half concentric

ellipses, and counting the number of *kal1*+ neoblasts in each section. Sections were evaluated according to their position compared to major landmarks (*bmp4* expressing muscle cells, DV boundary epidermal cells, and the intestine). The number of *kal1*+ cells in irradiated and unirradiated *bmp4* RNAi animals and controls was quantified by taking prepharyngeal images (400 μm^2, 10 confocal slices, Fig 6H–I) for all animals in four groups (irradiated control, unirradiated control, irradiated *bmp4* RNAi, unirradiated *bmp4* RNAi). Then the file names of the images were randomized and the images were analyzed by a different researcher. Positive cells were counted using the "Cell Counter" component in ImageJ, and documented for each file. Following measurements, the file names were derandomized, and data of different groups were compared.

Calculation of the overlap fraction in epidermal progenitors—Overlap fraction was calculated for *ovo-2* as follows: [Number of *ovo-2*+ cells expressing gene X/Number of *ovo-2*+ cells], where gene X represents any gene in the transcriptome for which gene expression was greater than $\log_2$(CPM+1) of 5. Overlap fraction for DCLK2 was calculated similarly. Genes expressed in a small fraction of the entire cell population (<25%) were removed as their overlap fraction was minor. Genes expressed throughout the cell population (> 66%) were also removed, to avoid confounding the results with genes expressed abundantly, such as housekeeping genes.

Phylogenetic analysis of epidermal genes—Phylogenetic analysis of *PRDM1-1*, *ovo-2,* and *ovo-3* was done by multiple alignment of the protein sequences with known sequences from representative model organisms using mafft v7.017b (Katoh et al., 2009) with flag [--auto]. Then gap sequences were trimmed, and trees resolved using RAxML (Stamatakis, 2006) with flags [Substitution model: PROTCAT DAYHOFF; Matrix name: DAYHOFF; Bootstrap: 100]. *kal-1* analysis was done using multiple methods: (1) Reciprocal BLASTP search [e-value < 1E-30) against the human proteome resulted in best similarity with KAL1; (2) Conserved protein domain analysis using CDART (Geer et al., 2002) and InterProScan v5.18-57.0 (Jones et al., 2014) of domain structure in model organisms and *S. mediterranea*; and (3) Classification based on the PANTHER database prediction using the protein sequence of the predicted planarian *kal1* (Mi et al., 2016).

QUANTIFICATION AND STATISTICAL ANALYSIS

Statistical analysis was performed using R v3.2.3. Unless stated otherwise, Student's t-test was used followed by Bonferroni correction for multiple hypothesis testing where applicable.

DATA AND SOFTWARE AVAILABILITY

RNA sequencing data generated in this study were deposited to SRA and is available under accession PRJNA353867 (http://www.ncbi.nlm.nih.gov/bioproject/353867).

Supplementary Material

Refer to Web version on PubMed Central for supplementary material.

Acknowledgments

We thank Kellie Kravarik and the Reddien lab members for manuscript comments. OW was supported by an EMBO long-term fellowship, and is the Howard Hughes Medical Institute Fellow of The Helen Hay Whitney Foundation. We acknowledge NIH (R01GM080639) support. PWR is a Howard Hughes Medical Institute Investigator and an associate member of the Broad Institute of Harvard and MIT.

References

Adell T, Salo E, Boutros M, Bartscherer K. *Smed-Evi/Wntless* is required for beta-catenin-dependent and -independent processes during planarian regeneration. Development. 2009; 136:905–910. [PubMed: 19211673]

Adler CE, Sanchez Alvarado A. Types or States? Cellular Dynamics and Regenerative Potential. Trends Cell Biol. 2015; 25:687–696. [PubMed: 26437587]

Adler CE, Seidel CW, McKinney SA, Sanchez Alvarado A. Selective amputation of the pharynx identifies a FoxA-dependent regeneration program in planaria. Elife. 2014; 3:e02238. [PubMed: 24737865]

Azimzadeh J, Wong ML, Downhour DM, Sanchez Alvarado A, Marshall WF. Centrosome loss in the evolution of planarians. Science. 2012; 335:461–463. [PubMed: 22223737]

Baxendale S, Davison C, Muxworthy C, Wolff C, Ingham PW, Roy S. The B-cell maturation factor Blimp-1 specifies vertebrate slow-twitch muscle fiber identity in response to Hedgehog signaling. Nature Genetics. 2004; 36:88–93. [PubMed: 14702044]

Camacho C, Coulouris G, Avagyan V, Ma N, Papadopoulos J, Bealer K, Madden TL. BLAST+: architecture and applications. BMC Bioinformatics. 2009; 10:421. [PubMed: 20003500]

Cibois M, Luxardi G, Chevalier B, Thome V, Mercey O, Zaragosi LE, Barbry P, Pasini A, Marcet B, Kodjabachian L. BMP signalling controls the construction of vertebrate mucociliary epithelia. Development. 2015; 142:2352–2363. [PubMed: 26092849]

Cowles MW, Brown DD, Nisperos SV, Stanley BN, Pearson BJ, Zayas RM. Genome-wide analysis of the bHLH gene family in planarians identifies factors required for adult neurogenesis and neuronal regeneration. Development. 2013; 140:4691–4702. [PubMed: 24173799]

Dubaissi E, Papalopulu N. Embryonic frog epidermis: a model for the study of cell-cell interactions in the development of mucociliary disease. Dis Model Mech. 2011; 4:179–192. [PubMed: 21183475]

Duncan EM, Chitsazan AD, Seidel CW, Sanchez Alvarado A. Set1 and MLL1/2 Target Distinct Sets of Functionally Different Genomic Loci In Vivo. Cell Reports. 2015; 13:2741–2755. [PubMed: 26711341]

Eisenhoffer GT, Kang H, Sanchez Alvarado A. Molecular analysis of stem cells and their descendants during cell turnover and regeneration in the planarian *Schmidtea mediterranea*. Cell Stem Cell. 2008; 3:327–339. [PubMed: 18786419]

Forsthoefel DJ, James NP, Escobar DJ, Stary JM, Vieira AP, Waters FA, Newmark PA. An RNAi screen reveals intestinal regulators of branching morphogenesis, differentiation, and stem cell proliferation in planarians. Developmental cell. 2012; 23:691–704. [PubMed: 23079596]

Gautier EL, Shay T, Miller J, Greter M, Jakubzick C, Ivanov S, Helft J, Chow A, Elpek KG, Gordonov S, et al. Gene-expression profiles and transcriptional regulatory pathways that underlie the identity and diversity of mouse tissue macrophages. Nature Immunol. 2012; 13:1118–1128. [PubMed: 23023392]

Geer LY, Domrachev M, Lipman DJ, Bryant SH. CDART: protein homology by domain architecture. Genome Res. 2002; 12:1619–1623. [PubMed: 12368255]

Glazer AM, Wilkinson AW, Backer CB, Lapan SW, Gutzman JH, Cheeseman IM, Reddien PW. The Zn finger protein Iguana impacts Hedgehog signaling by promoting ciliogenesis. Developmental Biology. 2010; 337:148–156. [PubMed: 19852954]

Gurley KA, Elliott SA, Simakov O, Schmidt HA, Holstein TW, Sanchez Alvarado A. Expression of secreted Wnt pathway components reveals unexpected complexity of the planarian amputation response. Developmental Biology. 2010; 347:24–39. [PubMed: 20707997]

Hayashi T, Asami M, Higuchi S, Shibata N, Agata K. Isolation of planarian X-ray-sensitive stem cells by fluorescence-activated cell sorting. Development, Growth & Differentiation. 2006; 48:371–380.

Jones P, Binns D, Chang HY, Fraser M, Li W, McAnulla C, McWilliam H, Maslen J, Mitchell A, Nuka G, et al. InterProScan 5: genome-scale protein function classification. Bioinformatics. 2014; 30:1236–1240. [PubMed: 24451626]

Katoh K, Asimenos G, Toh H. Multiple alignment of DNA sequences with MAFFT. Methods Mol Biol. 2009; 537:39–64. [PubMed: 19378139]

Lapan SW, Reddien PW. Transcriptome analysis of the planarian eye identifies *ovo* as a specific regulator of eye regeneration. Cell Reports. 2012; 2:294–307. [PubMed: 22884275]

Lavin Y, Winter D, Blecher-Gonen R, David E, Keren-Shaul H, Merad M, Jung S, Amit I. Tissue-resident macrophage enhancer landscapes are shaped by the local microenvironment. Cell. 2014; 159:1312–1326. [PubMed: 25480296]

Liu SY, Selck C, Friedrich B, Lutz R, Vila-Farre M, Dahl A, Brandl H, Lakshmanaperumal N, Henry I, Rink JC. Reactivating head regrowth in a regeneration-deficient planarian species. Nature. 2013; 500:81–84. [PubMed: 23883932]

Mi H, Poudel S, Muruganujan A, Casagrande JT, Thomas PD. PANTHER version 10: expanded protein families and functions, and analysis tools. Nucleic Acids Res. 2016; 44:D336–342. [PubMed: 26578592]

Molina MD, Neto A, Maeso I, Gomez-Skarmeta JL, Salo E, Cebria F. Noggin and noggin-like genes control dorsoventral axis regeneration in planarians. Current Biology : CB. 2011; 21:300–305. [PubMed: 21295481]

Molina MD, Salo E, Cebria F. The BMP pathway is essential for re-specification and maintenance of the dorsoventral axis in regenerating and intact planarians. Developmental Biology. 2007; 311:79–94. [PubMed: 17905225]

Orii H, Watanabe K. Bone morphogenetic protein is required for dorso-ventral patterning in the planarian Dugesia japonica. Development, Growth & Differentiation. 2007; 49:345–349.

Pearson BJ, Eisenhoffer GT, Gurley KA, Rink JC, Miller DE, Sanchez Alvarado A. Formaldehyde-based whole-mount in situ hybridization method for planarians. Developmental dynamics. 2009; 238:443–450. [PubMed: 19161223]

Petersen CP, Reddien PW. A wound-induced Wnt expression program controls planarian regeneration polarity. Proceedings of the National Academy of Sciences of the United States of America. 2009; 106:17061–17066. [PubMed: 19805089]

Picelli S, Bjorklund AK, Faridani OR, Sagasser S, Winberg G, Sandberg R. Smart-seq2 for sensitive full-length transcriptome profiling in single cells. Nature Methods. 2013; 10:1096–1098. [PubMed: 24056875]

Picelli S, Faridani OR, Bjorklund AK, Winberg G, Sagasser S, Sandberg R. Full-length RNA-seq from single cells using Smart-seq2. Nature Protocols. 2014; 9:171–181. [PubMed: 24385147]

Quigley IK, Stubbs JL, Kintner C. Specification of ion transport cells in the Xenopus larval skin. Development. 2011; 138:705–714. [PubMed: 21266406]

Reddien PW. Constitutive gene expression and the specification of tissue identity in adult planarian biology. Trends in Genetics : TIG. 2011; 27:277–285. [PubMed: 21680047]

Reddien PW. Specialized progenitors and regeneration. Development. 2013; 140:951–957. [PubMed: 23404104]

Reddien PW, Bermange AL, Kicza AM, Sanchez Alvarado A. BMP signaling regulates the dorsal planarian midline and is needed for asymmetric regeneration. Development. 2007; 134:4043–4051. [PubMed: 17942485]

Reddien PW, Oviedo NJ, Jennings JR, Jenkin JC, Sanchez Alvarado A. SMEDWI-2 is a PIWI-like protein that regulates planarian stem cells. Science. 2005; 310:1327–1330. [PubMed: 16311336]

Reddien PW, Sanchez Alvarado A. Fundamentals of planarian regeneration. Annual Review of Cell and Developmental Biology. 2004; 20:725–757.

Robinson MD, McCarthy DJ, Smyth GK. edgeR: a Bioconductor package for differential expression analysis of digital gene expression data. Bioinformatics. 2010; 26:139–140. [PubMed: 19910308]

Rouhana L, Weiss JA, Forsthoefel DJ, Lee H, King RS, Inoue T, Shibata N, Agata K, Newmark PA. RNA interference by feeding in vitro-synthesized double-stranded RNA to planarians: methodology and dynamics. Developmental dynamics. 2013; 242:718–730. [PubMed: 23441014]

Sanchez Alvarado A, Yamanaka S. Rethinking differentiation: stem cells, regeneration, and plasticity. Cell. 2014; 157:110–119. [PubMed: 24679530]

Satija R, Farrell JA, Gennert D, Schier AF, Regev A. Spatial reconstruction of single-cell gene expression data. Nature Biotechnology. 2015; 33:495–502.

Schindelin J, Arganda-Carreras I, Frise E, Kaynig V, Longair M, Pietzsch T, Preibisch S, Rueden C, Saalfeld S, Schmid B, et al. Fiji: an open-source platform for biological-image analysis. Nature Methods. 2012; 9:676–682. [PubMed: 22743772]

Scimone ML, Kravarik KM, Lapan SW, Reddien PW. Neoblast specialization in regeneration of the planarian *Schmidtea mediterranea*. Stem Cell Reports. 2014a; 3:339–352. [PubMed: 25254346]

Scimone ML, Lapan SW, Reddien PW. A forkhead transcription factor is wound-induced at the planarian midline and required for anterior pole regeneration. PLoS Genetics. 2014b; 10:e1003999. [PubMed: 24415944]

Scimone ML, Srivastava M, Bell GW, Reddien PW. A regulatory program for excretory system regeneration in planarians. Development. 2011; 138:4387–4398. [PubMed: 21937596]

Stamatakis A. RAxML-VI-HPC: maximum likelihood-based phylogenetic analyses with thousands of taxa and mixed models. Bioinformatics. 2006; 22:2688–2690. [PubMed: 16928733]

Tazaki A, Kato K, Orii H, Agata K, Watanabe K. The body margin of the planarian *Dugesia japonica*: characterization by the expression of an intermediate filament gene. Dev Genes Evol. 2002; 212:365–373. [PubMed: 12203092]

Trost A, Bauer JW, Lanschutzer C, Laimer M, Emberger M, Hintner H, Onder K. Rapid, high-quality and epidermal-specific isolation of RNA from human skin. Exp Dermatol. 2007; 16:185–190. [PubMed: 17286810]

Tu KC, Cheng LC, HTKV, Lange JJ, McKinney SA, Seidel CW, Sanchez Alvarado A. Egr-5 is a post-mitotic regulator of planarian epidermal differentiation. Elife. 2015; 4:e10501. [PubMed: 26457503]

van der Maaten L, Hinton G. Visualizing data using t-SNE. The Journal of Machine Learning Research. 2008; 9:85.

van Wolfswinkel JC, Wagner DE, Reddien PW. Single-cell analysis reveals functionally distinct classes within the planarian stem cell compartment. Cell Stem Cell. 2014; 15:326–339. [PubMed: 25017721]

Vij S, Rink JC, Ho HK, Babu D, Eitel M, Narasimhan V, Tiku V, Westbrook J, Schierwater B, Roy S. Evolutionarily ancient association of the FoxJ1 transcription factor with the motile ciliogenic program. PLoS Genetics. 2012; 8:e1003019. [PubMed: 23144623]

Wagner DE, Wang IE, Reddien PW. Clonogenic neoblasts are pluripotent adult stem cells that underlie planarian regeneration. Science. 2011; 332:811–816. [PubMed: 21566185]

Wenemoser D, Reddien PW. Planarian regeneration involves distinct stem cell responses to wounds and tissue absence. Developmental Biology. 2010; 344:979–991. [PubMed: 20599901]

Witchley JN, Mayer M, Wagner DE, Owen JH, Reddien PW. Muscle cells provide instructions for planarian regeneration. Cell Reports. 2013; 4:633–641. [PubMed: 23954785]

Wurtzel O, Cote LE, Poirier A, Satija R, Regev A, Reddien PW. A Generic and Cell-Type-Specific Wound Response Precedes Regeneration in Planarians. Developmental Cell. 2015; 35:632–645. [PubMed: 26651295]

Zhu SJ, Hallows SE, Currie KW, Xu C, Pearson BJ. A *mex3* homolog is required for differentiation during planarian stem cell lineage development. Elife. 2015; 4:e07025.

Highlights

- Single-cell RNA sequencing reveals spatial patterning in a progenitor pool.
- Planarian epidermal neoblasts read their position in the animal.
- Position-specific transcriptional programs in progenitors generate cell-type diversity.
- Patterning signals from muscle regulate epidermal neoblast positional identity.

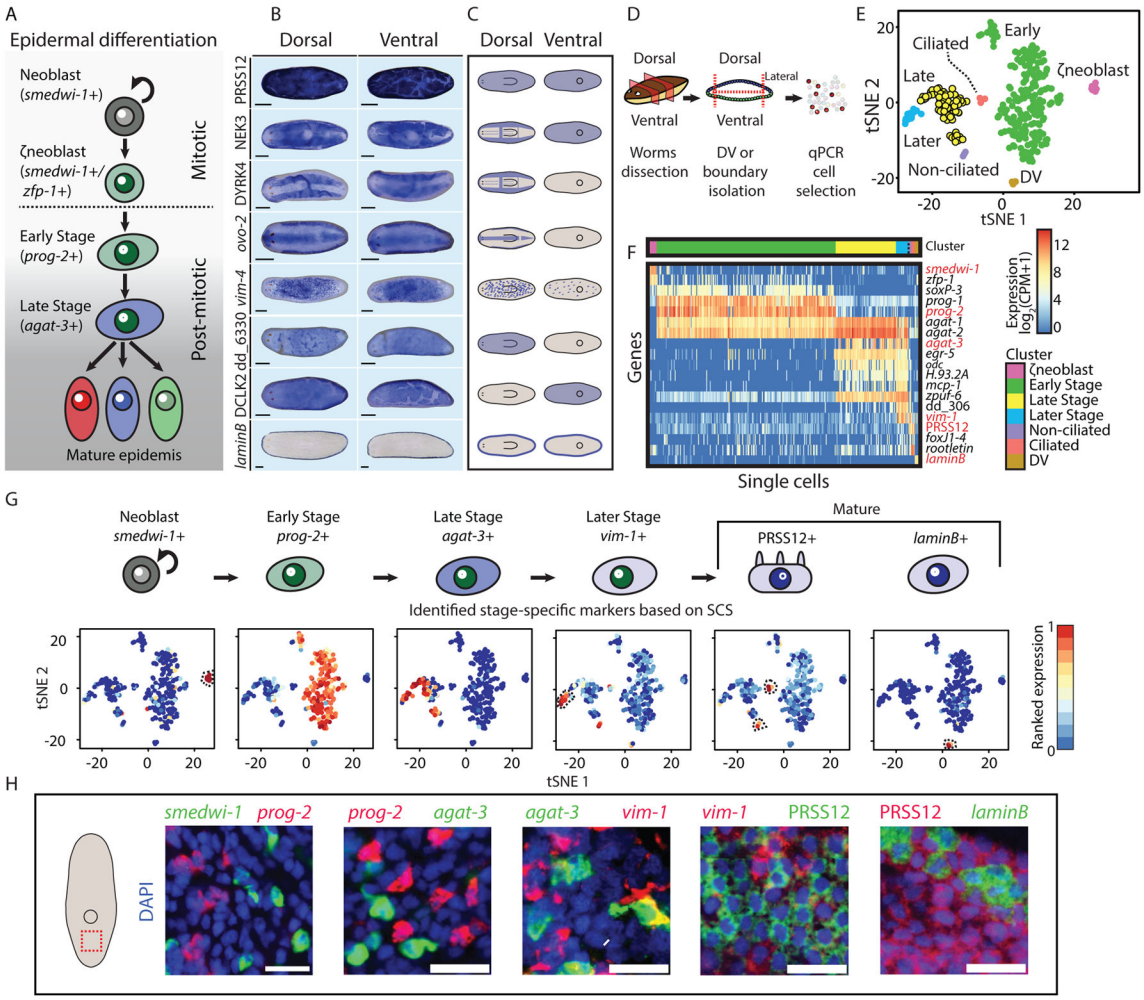

Figure 1. Mature epidermal identities revealed by RNA-seq

(A) A model for planarian epidermal maturation. Epidermal progenitors have spatiotemporally distinct stages (Eisenhoffer et al., 2008; Tu et al., 2015). Stage-specific gene expression markers distinguish different maturation stages. Epidermal progenitors generate multiple epidermal cell types characterized by different spatial distribution and gene expression. (B) Different epidermal gene expression patterns were detected by WISH. Shown are eight representative expression patterns (blue) in dorsal (left column) and ventral (right column) views. As animals are semitransparent, following bleaching (Pearson et al., 2009), assessing domains of expression requires examination from multiple viewpoints (scale bar = 100 μm). (C) Cartoon of the expression patterns reported in Fig 1B. Blue color represents region of epidermal expression. (D) Analysis of the epidermal lineage by SCS. Isolation of epidermal progenitors; pre-pharyngeal fragments were dissected to isolate dorsal, ventral, or lateral fragments, separately (STAR Methods). Tissues were disassociated and individual cells were sorted to plates by FACS. *agat-1* expression (Eisenhoffer et al., 2008) was measured by qPCR and cells expressing *agat-1* were sequenced and used for analysis, in combination with previously published SCS of the epidermal lineage (Wurtzel et al., 2015). (E) t-distributed stochastic neighbor embedding (tSNE) representation of

epidermal cells (dots) is shown (STAR Methods). Colors represent different clusters, with labels for cluster identities based on gene expression markers for epidermal maturation stages (Tu et al., 2015). (F) Gene expression in single cells (columns) of previously described epidermal genes (rows). Gene expression is represented by color (blue to red, low to high expression; counts per million, CPM; Hierarchal clustering was used to order cells within a cluster). Red labels denote genes that were subsequently used for FISH experiments, because of their power to discriminate between clusters, and their low background expression in FISH (Table S3). (G) Upper panel: Cluster-specific gene expression markers that were used for evaluating the distribution of epidermal lineage progenitors in situ. Markers were selected based on their fold-enrichment and power to discriminate between clusters. Lower panel: tSNE plot of cells (dots) colored by the ranked expression of the gene markers we selected across all sequenced cells (blue to red, low to high gene expression, respectively; dotted black line highlights cell clusters). (H) The selected gene expression markers were assessed by co-expression FISH analysis (scale bar = 20 μm). The markers had a nearly complete lack of co-expression, therefore permitting the analysis of distinct maturation stages.

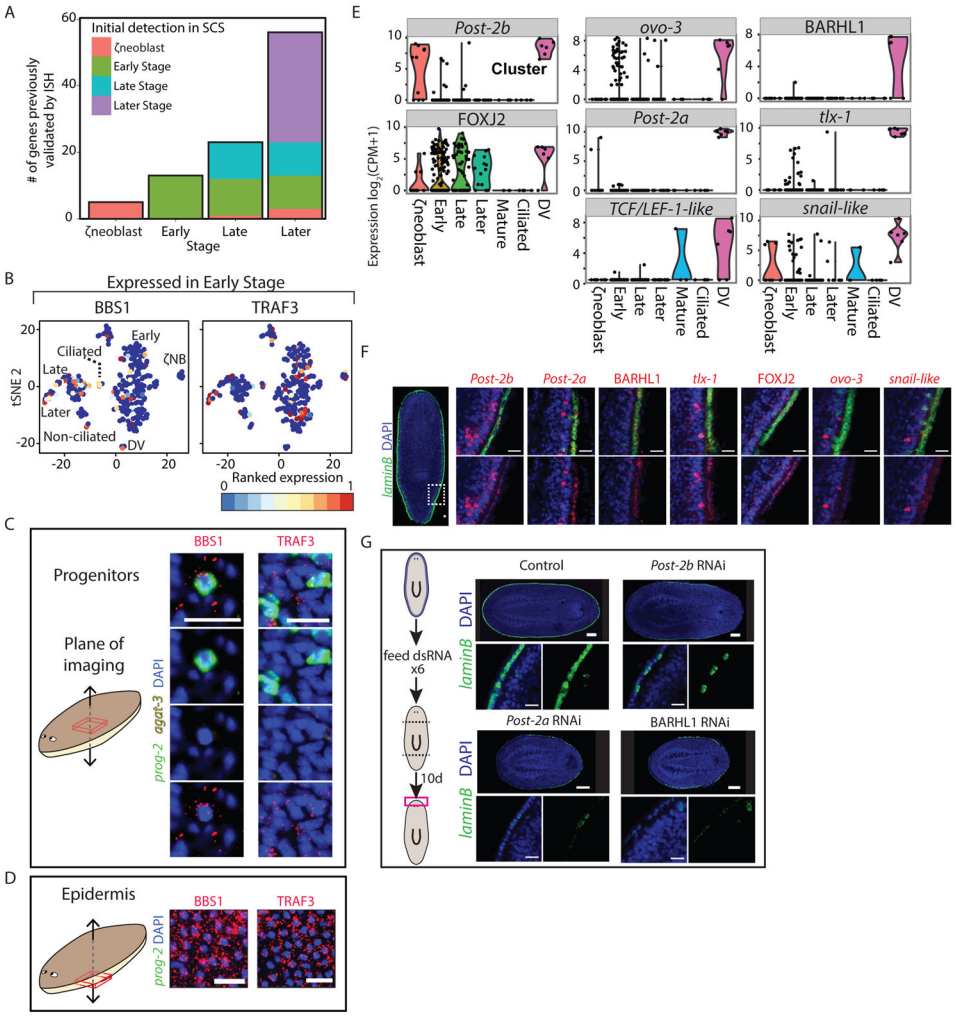

Figure 2. Mature epidermal gene expression is abundant in epidermal progenitors

(A) Expression of validated epidermal genes in SCS data across epidermal clusters. Shown are genes that were expressed only in the epidermal lineage. Color coding corresponds to the maturation stage in which the gene was initially expressed. (B) tSNE plots of two epidermal genes validated by WISH (BBS1 and TRAF3), that were found to be expressed in Early Stage progenitor cells (expression low to high, blue to red, respectively). (C–D) FISH validation of epidermal gene expression in Early Stage and Late Stage progenitors (C) and in mature epidermis (D), taken in different focal planes in the same animals (see schematic) by confocal microscopy (scale bar = 20 μm). White arrows indicate co-expression. Early Stage (*prog-2*) and Late Stage (*agat-3*) progenitor markers are not expressed in the mature epidermis. (E) Violin plots of the eight TFs that were enriched in the DV boundary epidermal cells are shown. Black dots represent expression of a single cell. (F) FISH validation of DV-boundary epidermis TFs, including co-expression with *laminB*. The expression of the TFs is shown in higher magnification at a DV region corresponding to the white-dashed box in the overview (left) image. See also Fig S3G. Scale bar = 20 μm. (G) Inhibition of three of the DV epidermal boundary TFs led to a reduction in DV epidermal boundary gene expression in regenerating animals 10 days following amputation, as

observed by FISH for *laminB* expression. Top panels: The expression of *laminB* is greatly reduced in the perturbed animals. Scale bar = 100 μm. Bottom panels: Higher magnification of the DV boundary in the different RNAi conditions. Scale bar = 20 μm.

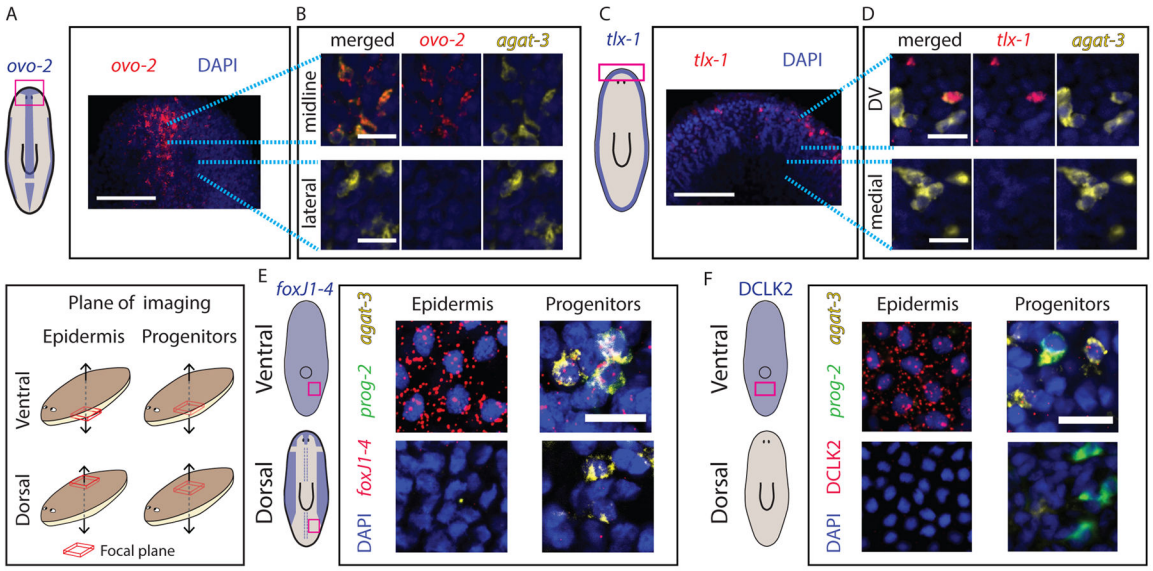

Figure 3. Expression of spatially-restricted mature epidermal identities is pre-patterned in epidermal progenitors

(A) *ovo-2* expression in the head is restricted to the midline (Scale bar = 100 μm; schematic shows spatial expression restriction in blue). (B) In the focal plane of the progenitors, *ovo-2* expression is limited to progenitors in the midline (upper panel), and is not found in progenitors immediately lateral to the midline (lower panel). Blue dotted lines indicate higher magnification area. Scale bar = 20 μm. (C) *tlx-1* expression in mature epidermis is found in DV epidermal cells (left schematic), however, *tlx-1* expression was also detectable in epidermal progenitors in proximity to the DV boundary, but not detected in progenitors in other parts of the animal (scale bar = 20 μm). (E–F) Shown are confocal images at different focal planes of dorsal or ventral regions of the animal. See key (left panel). Scale bar = 20 μm. (E) *foxJ1-4*, an essential gene for ciliogenesis (Vij et al., 2012) is expressed in ventral epidermis (top-left), and the lateral flanks the dorsal epidermis, but not in the dorsal-medial part (bottom-left; See schematic). The expression of *foxJ1-4* is present in epidermal progenitors at the ventral region (top-right), but not in the dorsal region (bottom-right). (F) The expression of DCLK2 is detectable in ventral but not dorsal epidermis (Fig 1B; left schematic). Similarly, ventral epidermal progenitors, but not dorsal progenitors already displayed DCLK2 expression, demonstrating that epidermal progenitors activate region-appropriate transcriptional program according to their DV position.

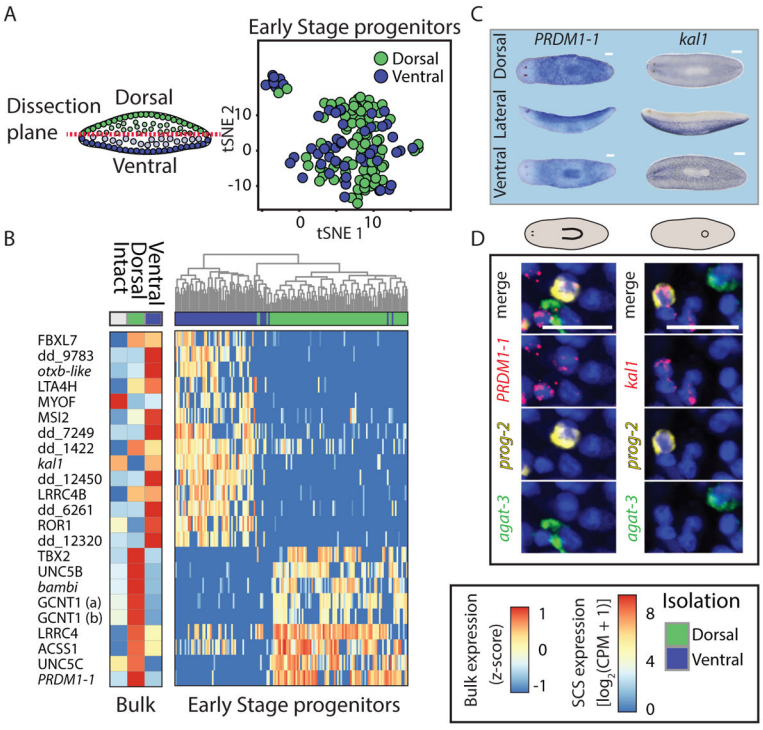

Figure 4. Early Stage progenitors activate divergent transcriptional programs based on their DV location

(A) Left: Tissues were dissected from dorsal and ventral regions and epidermal progenitors were isolated by FACS and qPCR (Fig 1D; STAR Methods). Early Stage progenitors were identified computationally (STAR Methods), and gene expression of dorsal and ventral Early Stage progenitor samples was compared. Right: tSNE plot of Early Stage progenitors from dorsal and ventral regions (green and blue dots, dorsal and ventral cells, respectively). (B) Right: Differentially expressed genes (rows) in dorsal and ventral Early Stage progenitors (columns) demonstrate differences between cells that differ in their position across the boundary. Dendrogram was generated by hierarchical clustering of the gene expression. Many of the genes that have a biased DV-expression in the progenitors also display biased expression in the mature epidermis-enriched samples (left heat map; shown is the average expression across replicates from the same sample type). (C) WISH analyses of the dorsal-specific gene marker (*PRDM1-1*) and the ventral-specific gene marker (*kal1*) demonstrate distinct regionalized expression (scale bar = 100 μm). (D) Expression of *PRDM1-1* and *kal1* is found in Early Stage progenitors and is restricted to the dorsal or ventral regions, respectively. Shown is co-expression of either *PRDM1-1* or *kal1* with an Early Stage marker (*prog-2*; white arrow).

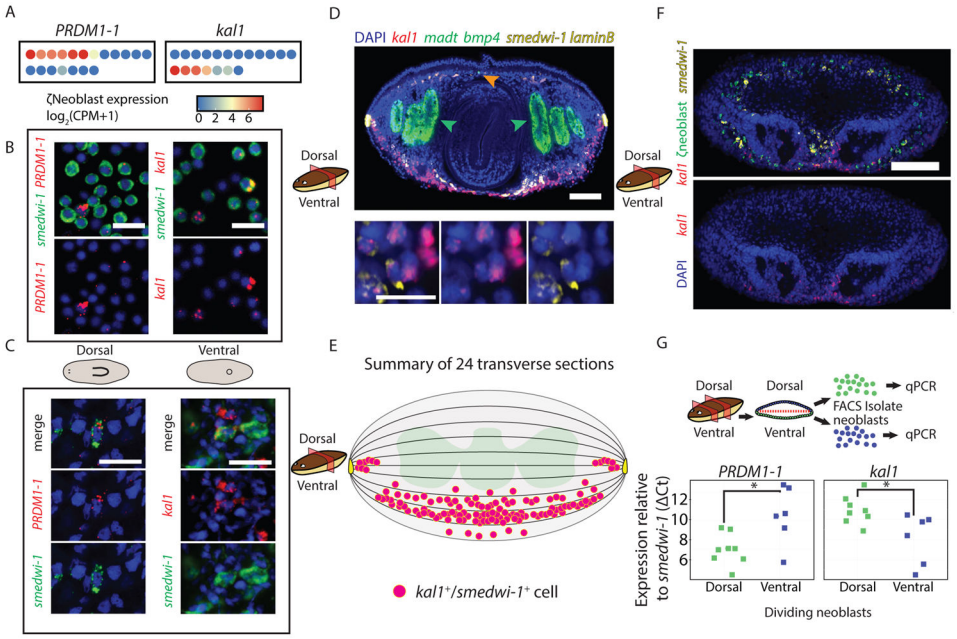

Figure 5. Spatially opposed expression of *PRDM1-1* and *kal1* in neoblasts

(A) ζneoblasts express *PRDM1-1* or *kal1* in mutually exclusive single ζneoblasts (dots; blue to red, low to high gene expression, respectively). (B) The fraction of neoblasts expressing dorsal (*PRDM1-1*) or ventral (*kal1*) markers was estimated by co-expression analysis of FACS-isolated dividing neoblasts, and co-staining with a neoblast marker (*smedwi-1*). (C) FISH showing *PRDM1-1* expression in dorsal neoblasts (left), and *kal1* is found only in ventral neoblasts (right). *kal1* was not expressed in dorsal neoblasts in at least 10 animals; *PRDM1-1* was not expressed in ventral neoblasts in at least 10 animals. (D) Shown is a transverse section (see cartoon) labeled for *kal1* (red), madt (green; intestinal marker; green arrows), *bmp4* (green; orange arrow), *smedwi-1* (yellow; neoblast marker), and *laminB* (yellow; DV-boundary epidermis). Scale bar = 100 μm. *kal1*+/*smedwi-1*+ cells were counted (bottom panel, white arrows) and their position in the animal was documented (STAR Methods). Scale bar = 20 μm. See also Fig S6E. (E) Summary of the location of *kal1*+/*smedwi-1*+ cells in 24 transverse sections (magenta circles). Sections were divided to 10 regions (bounded by black lines) and the number of *kal1*+/*smedwi-1*+ cells was counted in each region (STAR Methods). The medial-lateral position of the cells was not measured and the medial-lateral spread is for clarity, except for cells next to the DV-boundary epidermis (yellow cartoon), which represent the approximate distance of these cells from the boundary. All *kal1*+/*smedwi-1*+ cells were ventral to the intestine (green cartoon), except for those next to the DV-boundary epidermis. (F) FISH on animals labeled for ζneoblasts markers (pool of *soxP-3* and *zfp-1*) and *kal1* shows that *kal1*-ζneoblasts extends more internally than *kal1* expression (white arrow), suggesting that ventral ζneoblasts express *kal1* when they are only near the epidermal surface. Top panel shows all channels; bottom panel shows *kal1* expression and DAPI. Scale Bar = 100 μm. See Figure S6F for single channel images. (G) Top panel: Schematic of dividing neoblast isolation by FACS (STAR Methods). Pre-pharyngeal segments were isolated and were dissected into dorsal and ventral fragments. The fragments were macerated, separately, and cells (green and blue dots, dorsal and ventral

cells, respectively) were isolated by FACS into groups of 500 cells (STAR Methods; eight dorsal samples and six ventral samples). The samples were processed (STAR Methods) and; bottom panel: tested by qPCR for the expression of *PRDM1-1* and *kal1*, with their expression normalized by *smedwi-1* expression (green and blue squares represent 500-cell samples, dorsal or ventral, respectively). Significance of difference in expression was tested by Student's t-test and corrected for multiple hypothesis testing using Bonferroni correction. Overlaid are 95% bootstrap-calculated confidence intervals.

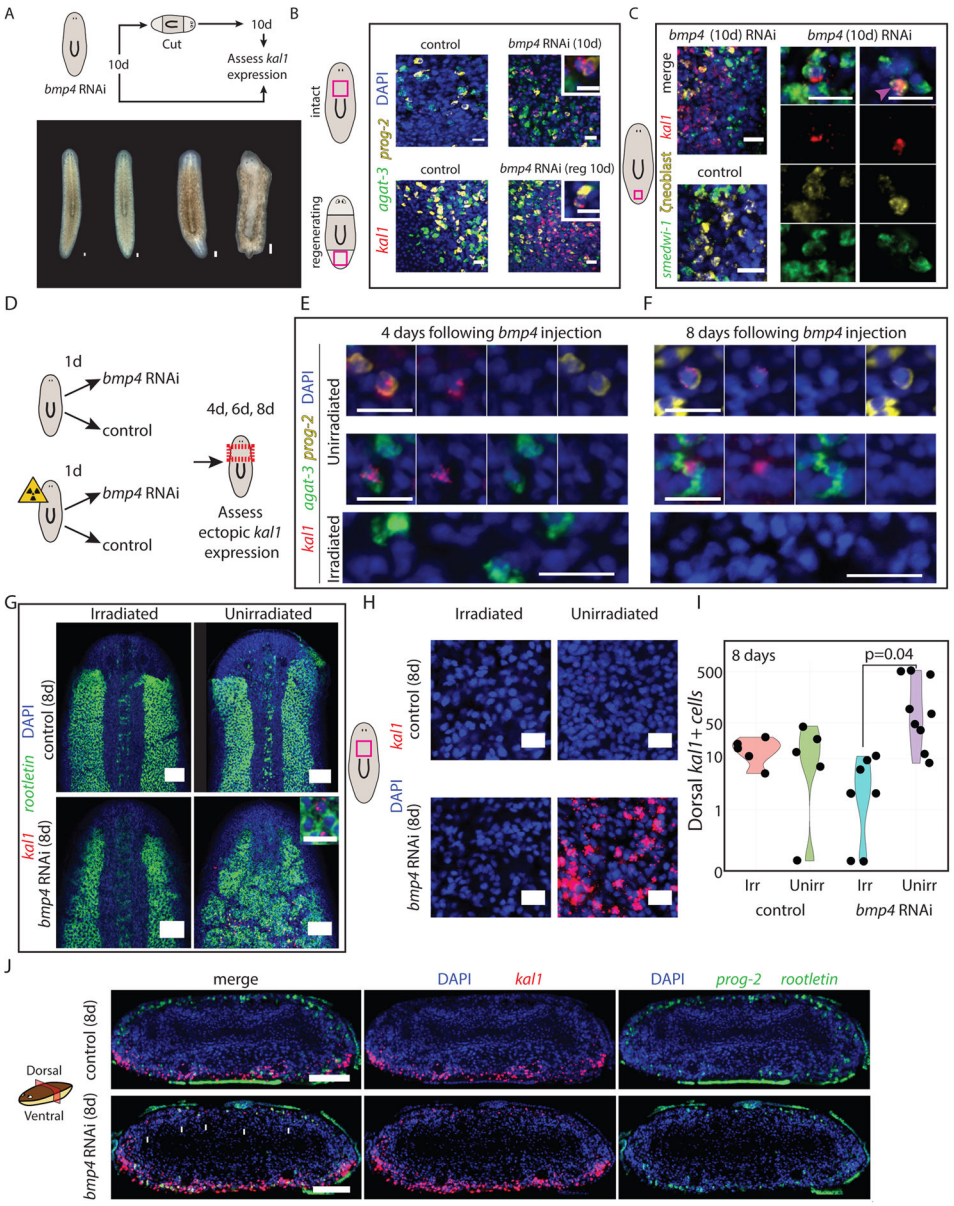

Figure 6. Planarian ζneoblast gene expression is regulated by extracellular positional signaling

(A) *bmp4* was inhibited by RNAi (STAR Methods), and 10 days following the first feeding of three, animals were either fixed or cut and allowed to regenerate for 10 days (upper panel). Animals did not have any visible defects prior to cutting (bottom panel), but following cutting and regeneration, they displayed major morphological defects, as previously reported (Molina et al., 2007; Reddien et al., 2007). (B) *kal1* expression was observed 10 days following *bmp4* RNAi on the dorsal surface, but never in control animals. Shown are animals before cutting (top) and animals at 10 day following regeneration (labeled reg 10d). Insets show a dorsal cell in *bmp4* RNAi animal that co-expresses an Early Stage marker (*prog-2*) and *kal1*, demonstrating that reduction in BMP expression is sufficient for the appearance of ventral markers dorsally. Inset scale bar = 10 μm. (C) *kal1* expression is observed in dorsal ζneoblasts, suggesting that ζneoblasts sense *bmp4*

expression in their environment and specify their positional gene expression accordingly. At day 10 following *bmp4* inhibition animals displayed *kal1* expression dorsally (left panel). Middle panel: In *bmp4* RNAi animals, we detected dorsal *kal1*+ cells that also express *smedwi-1* (a pan-neoblast marker), and ζneoblast markers (combination of *soxP-3* and *zfp-1*, (van Wolfswinkel et al., 2014)), indicating that they were indeed epidermal neoblasts (white arrow). Right panel: In addition, we identified *kal1*+/ζneoblast+ cells that did not express *smedwi-1*, suggesting that they are more differentiated epidermal progenitors. Scale bar = 20 μm. (D) Animals were divided into two cohorts, one of which was lethally irradiated on day zero; the other was unperturbed. Half of the animals each cohort received a single injection of either *bmp4* dsRNA or a control dsRNA. Animals were fixed and analyzed at day four, day six and day eight following injection. (E–F) At days four and eight following *bmp4* dsRNA injections, epidermal progenitors on the dorsal side (*prog-2*+ or *agat-3*+ cells, top and middle panels, respectively), which expressed *kal1*, were detectable. Conversely, *kal1*+ dorsal epidermal progenitors were not detected in irradiated animals. At day eight following irradiation, epidermal progenitors are completely ablated. See also Fig S7A. Scale bar = 20 μm. (G) The dorsal expression of *rootletin* in the irradiated *bmp4* animals is indistinguishable from control animals. Conversely, in three of eight unirradiated *bmp4* RNAi animals, the dorsal *rootletin* expression resembled the ventral surface of the animal. See Fig S7B. Scale bar = 100 μm. Inset shows *rootletin*+ cells expressing *kal1*. Inset scale bar = 20 μm. (H) Expression of *kal1* in dorsal pre-pharyngeal regions. Only unirradiated *bmp4* RNAi had dorsal expression. Scale bar = 20 μm. (I) Quantification of the number of *kal1*+ cells on the pre-pharyngeal dorsal region of each animal (black dot) analyzed. Significance was assessed using Student's t-test. Groups labeled Irr and Unirr represent irradiated and unirradiated groups, respectively. (J) Transverse section showing the spatial distribution of *kal1*+ cells in control and *bmp4* RNAi animals. *kal1*+ cells were never found in the middle of the animal, despite ectopic expression in all *bmp4* RNAi sections analyzed (white arrows). Scale bar = 100 μm.

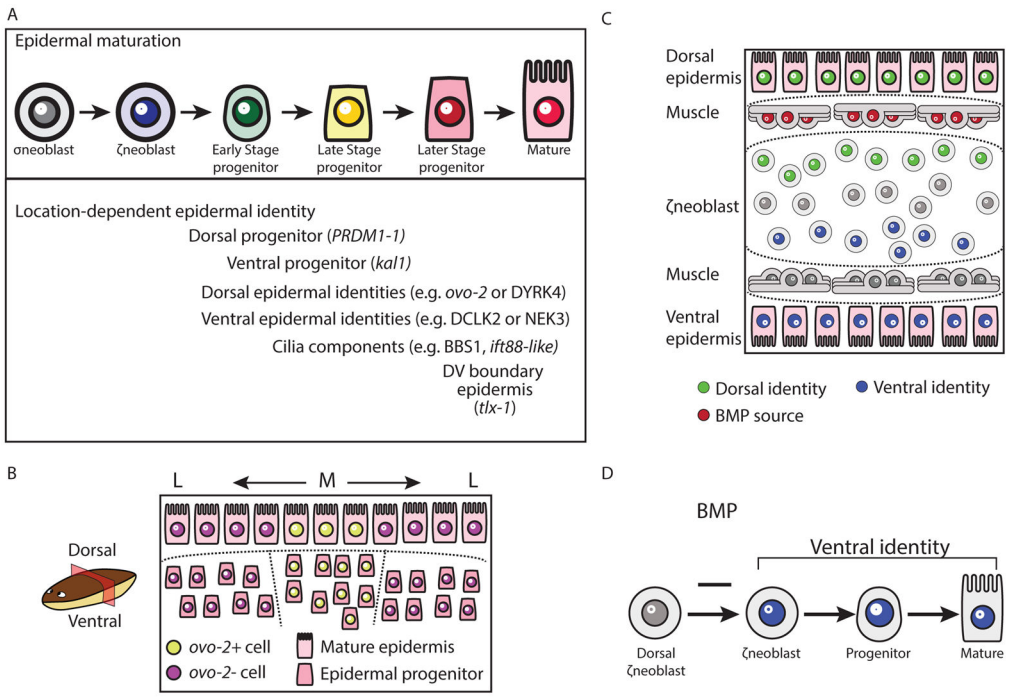

Figure 7. Model for planarian epidermal differentiation

(A) Top panel: Planarian epidermal cells mature in a spatiotemporally defined sequence, in which progenitors go through several transitions defined by cellular morphology and spatial distribution. Bottom panel: Genes that are associated with distinct epidermal identities are expressed in all stages of the epidermal maturation, in a spatially-defined manner. Some of these genes are already expressed in ζneoblasts suggesting that ζneoblasts sense their position in the animal. (B) Some spatially-restricted epidermal identities are pre-patterned in epidermal progenitors. The model presents a view of a transverse cross-section. Dorsal is up. Medial mature epidermal cells (M; Large shapes) express *ovo-2* (yellow nuclei), whereas lateral cells do not (L; purple nuclei). FISH analysis of epidermal progenitors determined that epidermal progenitors near the midline already express *ovo-2* (yellow), whereas lateral epidermal progenitors do not (purple). (C) The specification of ζneoblasts to ventral (*kal1+*) identities is repressed by *bmp4* expression from dorsal muscle cells (red elongated cells). ζneoblasts, which are in proximity to the BMP source, can express dorsal markers (*PRDM1-1+*; green circles), which is correlated with the emergence of additional dorsal epidermal identities. By contrast, cells that are far from the BMP source can specialize to ventral progenitors (*kal1+*; blue circles), which are associated with ventral epidermal identities. Inhibition of BMP signaling results in the emergence of *kal1+* ζneoblasts dorsally. (D) BMP inhibits the expression of genes associated with a ventral identity in dorsal ζneoblasts. Inhibition of BMP leads to emergence of ventral identities dorsally.